

CUSTOMIZED AND MODULAR CONTROL OF
GENE EXPRESSION FOR PRECISION GENE
THERAPIES

Thesis by
Acacia Michelle Hori Mayfield

In Partial Fulfillment of the Requirements for the Degree of
Doctor of Philosophy in Bioengineering

The Caltech logo, featuring the word "Caltech" in a bold, orange, sans-serif font, centered within a light orange rectangular background.

CALIFORNIA INSTITUTE OF TECHNOLOGY
Pasadena, California

2024
(Defended May 28, 2024)

© 2024

Acacia Michelle Hori Mayfield

ORCID: 0000-0001-7308-6480

ACKNOWLEDGEMENTS

It is with sincerest gratitude that I acknowledge those who have helped my scientific development along the way. I must first acknowledge Mark T. Hori, who taught me to wonder about the living world, and that when wondering alone does not satisfy the soul, the best next step is the practice of science. Without his influence, I would have become a miserable attorney.

I thank those who nurtured my inquisitiveness when others were discouraging of a young girl's endless questions and opinions: Linda McNeil and Xochitl Navamorenó. I thank those who taught me to write clearly, which in turn, taught me to think clearly: Drs. Judith Haut, Stacy Ordonez, Barbara Barnett, and Dan Segal.

I thank those who mentored me through my education in neuroscience and independent research: Drs. Melissa Coleman, Kerry Thompson, James Shorter, Michael Soo, Ben Deverman, Nick Goeden, Nick Flytzanis, Sripriya Kumar, Jennifer Treweek, Elliott Robinson, Collin and Rose Challis and Joseph Hacia. To my collaborators, Michael Flynn, Rongrong Du and Dr. Michael Elowitz: thank you for adding rigor to our work and improving my approach to science. To my G-Lab colleagues, thank you for your feedback, ideas, and help in improving my projects and having fun along the way: Gerry Coughlin and Drs. Yujie Fan, Máté Borsos, and Tim Shay. I also thank the MD-PhD program at USC-Caltech, for supporting my training plans and providing every opportunity to explore what it means to be a physician-scientist, especially Roland Rapanot and Drs. Brian Lee, Nuria Pastor-Soler, Mark Davis, and David Hinton. To my committee, Drs. Michael Elowitz, Henry Lester, and Mary Kennedy: thank you for your helpful advice, seasoned feedback, and overall support. And to Elisha Mackey and Pat Anguiano, none of my work would have been possible without your foundational support of all lab operations.

To the OLAR staff, especially Ana Colon, Nicole McMillan, Desiree Hernandez, Nathalie Tam, Luisa Iturbide and Syed Ahsan, who painstakingly cared for my fragile model animal lines, thank you for the hard work that you do to enable these types of projects with the highest standards of animal welfare in mind. To all my mice, thank you for your sacrifice. Your critical role in these

experiments is irreplaceable, and I hope that you felt respected in the pursuit of better understanding of biology and development of strategies to make genetic medicine safer for all.

I thank my mentees over the years, formal and informal, for teaching me how to teach and how to learn. Most of all I must acknowledge Anastasiya Grebin and Desmond Edwards for their contributions to our collective understanding of how our Friedreich's Ataxia and Rett Syndrome therapeutic candidates behave *in vivo*. And to Rana Eser and Karan Mahe, thank you for helping the work started here continue to evolve in new and exciting ways.

I thank those who, when life, science, and medicine interact in personal ways, anchor me to what truly matters in life. Drs. Cory Mayfield, Jessica Griffiths, Ravali Reddy, Timothy Williamson, Angad Gogia, Emily Chu, Krishan Patel, Emmanuelle Hodara, and Ms. Olivia Mayfield. I also thank the inaugural Board of the Women in BBE group for becoming a powerful support network that has made graduate school more fun and doable during turbulent times: Drs. Namita Sarraf, Jessica Griffiths, Rochelle Diamond, and Riley Galton. And to those who were advancing the status of women at Caltech long before the formation of this group, thank you for your advocacy, which has made the transition to parenthood much more attainable as a PhD student: Drs. Marianne Bronner, Mary Kennedy, Pamela Bjorkman, and Riley Galton.

Of course, no one has had a greater impact on my scientific development and professional trajectory, expanding opportunities for me and believing in my potential at times when my world felt very small, than my advisor, Dr. Viviana Gradinaru. She has given me the greatest gifts anyone can give a person: time and reagents, along with wise counsel when it comes to interpretation, priorities, and remembering to find the joy in all of it. Thank you for everything.

ABSTRACT

Genetic disorders are caused by mutations in essential genes that disturb the abundance or function of proteins, tipping cells and tissues from homeostatic harmony into disorder. Developing treatment for genetic diseases involves precision approaches, as gene therapies target the root causes of highly specific pathologic processes at the level of gene replacement, editing, or downstream compensation for a harmful genetic change. Safe access to these cell populations, and the ability to control the behavior of therapeutic cargo after delivery to target tissues, will enable the field to develop safe and effective therapies with the potential to be curative. Systemically delivered AAVs can noninvasively target therapeutic genetic cargo to diverse disease loci throughout the body, but at high doses required for therapeutic penetrance of naturally occurring serotypes, these vectors can cause severe toxicity, emphasizing the need for both targeted, efficient gene delivery vectors, and other means of transgene expression control. This work describes three examples of AAV capsid and cargo design strategies that seek to control where, when, and at what level therapeutic transgene expression can be achieved in a preclinical context. First, we utilize native putative regulatory elements to encourage physiologic level of ectopic frataxin expression in a mouse model of Friedreich's Ataxia, finding that when delivered to both the brain and peripheral nervous system, treatment prevents progression of motor and coordination deficits. Next, we utilize the genetic incoherent feedforward loop circuit motif at the RNA level to decouple vector delivery level from transgene expression level of MeCP2 in a mouse model of Rett Syndrome, finding that when regulated to near endogenous healthy levels of RNA, AAV-MeCP2-IFFL enables behavioral rescue without overexpression toxicity. Lastly, we employ the mechanism for AAV-genome stability *in vivo* to modulate expression using a post-hoc AAV administration. Together, these methods and applications demonstrate that modular and custom approaches can improve the precision, safety and efficacy problems that the gene therapy field needs in order to advance more treatments for rare disorders.

PUBLISHED CONTENT AND CONTRIBUTIONS – INCLUDED IN THESIS

Flynn MJ¹, Mayfield AMH¹, Du R, Gradinaru V, Elowitz MB. Synthetic dosage-compensating miRNA circuits allow precision gene therapy for Rett syndrome.

bioRxiv 2024.03.13.584179; doi: <https://doi.org/10.1101/2024.03.13.584179>

A.M. participated in the conception of the project and design of the in vivo portion of the study, including selection of viral vectors, tissue handling, and protein analysis, and evaluation of in vivo phenotypes. She also participated in the writing of the manuscript.

Coughlin GM, Borsos M, Appling N, Barcelona BH, Mayfield AMH, Mackey ED, Eser RA, Chen X, Kumar SR, Gradinaru V. Spatial genomics of AAVs reveals mechanism of transcriptional crosstalk that enables targeted delivery of large genetic cargo.

bioRxiv 2023.12.23.573214; doi: <https://doi.org/10.1101/2023.12.23.573214>

A.M. participated in gait analysis of mice in the cacna1a portion of the project, and conceived of the additional therapeutic applications of AAV genome crosstalk.

Hori AM, Grebin A, Robinson JE, Chen X, Flytzanis N, Goeden N, Chan K, Deverman B, Gradinaru V. Targeted gene therapy with engineered systemic AAVs for the central and peripheral nervous systems prevents motor coordination phenotypes in a mouse model of Friedreich's Ataxia. ASGCT Annual Meeting Abstracts, Molecular Therapy, Volume 29, Issue 4, Supplement 1, 2021, Pages 1-427, ISSN 1525-0016, <https://doi.org/10.1016/j.ymthe.2021.04.019>.

A.M. created the viral materials, designed and executed the behavioral experiments, collected and analyzed the data, and authored and presented this abstract and presentation.

Hori AM, Robinson JE, Chan K, Flytzanis N, Goeden N, Deverman B, Gradinaru V. Recombinant AAVs target custom frataxin therapeutic cassettes to tissues of pathophysiologic relevance in Friedreich's Ataxia. 2020 ASGCT Annual Meeting Abstracts, Molecular Therapy, Volume 28, Issue 4, Supplement 1, 2020, Pages 1-592, ISSN 1525-0016, <https://doi.org/10.1016/j.ymthe.2020.04.019>.

A.M. created viral materials, collected and analyzed brain tissue, and authored and presented this abstract and presentation.

Challis C, Hori A, Sampson TR, Yoo BB, Challis RC, Hamilton AM, Mazmanian SK, Volpicelli-Daley LA, Gradinaru V. Gut-seeded α -synuclein fibrils promote gut dysfunction and brain pathology specifically in aged mice. *Nature Neuroscience*. 2020 Mar;23(3):327-336. doi: 10.1038/s41593-020-0589-7. Epub 2020 Feb 17. PMID: 32066981; PMCID: PMC7065967.

A.M. performed revision animal behavior experiments for this publication, including data analysis, and authored the methods and results for these experiments.

TABLE OF CONTENTS

Acknowledgements.....	iii
Abstract	v
Published Content and Contributions.....	vi
Table of Contents.....	viii
Nomenclature and Abbreviations.....	ix
Chapter I: Background: Modular design elements to enable parallel development of safer precision gene therapies for disorders sharing pathophysiologic characteristics	12
Chapter II: Mimicking healthy patterns of endogenous expression through identification and incorporation of native regulatory elements.....	26
Chapter III: Delivery-agnostic expression regulation to circumvent overexpression toxicity in Rett Syndrome	49
Conclusion.....	91
Appendix A: Materials and Methods, Chapter II.....	92
Appendix B: Materials and Methods, Chapter III.....	95

NOMENCLATURE AND ABBREVIATIONS

AAV. Adeno-associated virus.

bp. Base pair (refers to DNA locus or length).

CAG. A strong promoter comprised of sequences from the cytomegalovirus early enhancer, chicken beta-actin promoter and rabbit beta-globin splice acceptor. Expresses ubiquitously.

Capsid. In this work, refers to the outer protein shell of an assembled AAV, which surrounds the cargo.

Cargo. In this work, refers to the DNA construct containing a transgene sequence, along with regulatory and targeting elements, positioned within a backbone of replication incompetent AAV genome.

CNS. Central nervous system. Comprised of neurons, glia, oligodendrocytes, astrocytes, and other subtypes of cells and tissues in the brain and spinal cord.

Concatamer. In this work, refers to an organized and functional assembly of multiple AAV genomes appended together within a single cell.

DNA. Deoxyribonucleic acid.

DRG. Dorsal root ganglion. Contains neuronal cell bodies and other cell types involved in sensory input and processing.

Ectopic. Gene or protein introduced from a vector.

Endogenous. Gene or protein expressed from the host genome.

FA. Friedreich's Ataxia.

FLAG. Epitope tag for immunohistochemistry.

FXN. Frataxin.

GD. Gaucher's Disease.

Gene Therapy. Genetically encoded transgenes introduced to a model organism or human patient in order to compensate for a pathologic genetic mutation or disease-causing deficit.

GFP; EGFP. Green fluorescent protein.

HCR. Hybridization chain reaction.

HEK293. Human embryonic kidney cells.

hiPSC. Human induced pluripotent stem cells.

IF. Immunofluorescence.

IHC. Immunohistochemistry.

ITR. Inverted terminal repeat.

MAP2. Antigenic marker found in mature neurons.

Motif. Modular genetic sequence.

NeuN. Antigenic marker found in mature neurons.

pAAV. Denotes DNA plasmid backbone that encodes an AAV genome.

PD. Parkinson's Disease.

PEG. Polyethylene glycol.

PFA. Paraformaldehyde.

PNS. Peripheral nervous system. Comprised of neurons and supportive cells located throughout the body, excluding those with cell bodies residing in the central nervous system. For example, sensory, sympathetic and parasympathetic neurons and ganglia in the dorsal root of the spinal cord, the sympathetic chain, and neurons in peripheral tissues, are all part of the peripheral nervous system.

RO. Retro-orbital route of administration.

shRNA. Small hairpin RNA.

Transduction. Expression of a transgene from a viral vector.

Transfection. Expression of a transgene from unpackaged DNA.

Chapter 1

BACKGROUND: MODULAR DESIGN ELEMENTS TO ENABLE PARALLEL DEVELOPMENT OF SAFER, PRECISION GENE THERAPIES FOR DISORDERS SHARING PATHOPHYSIOLOGIC CHARACTERISTICS

This chapter contains work from the following publications:

Challis C, Hori A, Sampson TR, Yoo BB, Challis RC, Hamilton AM, Mazmanian SK, Volpicelli-Daley LA, Gradinaru V. Gut-seeded α -synuclein fibrils promote gut dysfunction and brain pathology specifically in aged mice. *Nature Neuroscience*. 2020 Mar;23(3):327-336. doi: 10.1038/s41593-020-0589-7.

RARE GENETIC DISORDERS ARE COLLECTIVELY COMMON

There are roughly 30-40,000 protein-coding genes in the human genome, carrying out synergistic duties for cells in the dance of life (Lander 2001). Mutations in these genes that alter the balance required for healthy cellular function but are still compatible with life are thought to cause upwards of 7,000-8,000 distinct genetic disorders (Amberger 2015). As the body can tolerate some mutations more readily than others, there is vast variance in the incidences and prevalences of each of these, from one in a million patients to as common as one in several hundred. However uncommon a single diagnosis may be, when considered collectively, rare genetic disorders are much more common than the phrase would suggest. Even when restricting the definition of 'rare' to an incidence of less than 1 in 2,000 people, the total population of affected patients is estimated at upwards of 350 million individuals worldwide (Klimova 2017). Compared to the global burden of common diseases, the impact of rare diseases is surpassed only by cardiovascular disease, at an estimated 390 million individuals, and surpasses the total burden of cancer, affecting roughly 250 million people (Roser 2021).

A major challenge of treating genetic disorders is that unlike treatments for cardiovascular disease or cancer, each genetic disorder, and even each patient's pathologic mutation within the same

disorder, may vary so profoundly from the next that treatments developed for one subset of patients may not be usable for others. Gene therapy offers an opportunity to create customized medicine with a level of precision that may even be tailored to a specific patient's harbored mutation, but this level of precision comes at both an economic and temporal cost, that is intractable for developing therapies that are specific and efficacious for the rarest disorders. The biggest example of this is the curative therapy Glybera from uniQure, which was curative for familial lipoprotein lipase deficiency (incidence 1:250,000 worldwide) but was pulled from the market 5 years after approval due to cost for a small patient population (Senior 2017). More prevalent disorders such as spinal muscular atrophy (incidence 1:10,000) share the burden of high cost, but as its prevalence is much higher than fLPLD, not only is it the most successful gene therapy to be introduced, it is also creating an enormous burden of cost for individuals and nations with public health systems such as Brazil and leading to drug rationing (Robbins 2023).

Broadening the toolkit for developing these therapies can lead to effective and equitable treatments for disorders across the spectrum of rarity, and there are several ways to achieve this. Careful selection of upstream or downstream targets, as demonstrated in Challis et al. 2020, can utilize known biochemical relationships to expand the utility of gene therapy designs that may be more directly connected to lysosomal storage disorders such as Gaucher's Disease (GD) to more common applications such as Parkinson's Disease (PD). Because they share a biochemical pathway, introduction of glucocerebrosidase, the enzyme implicated in GD, was able to reduce phosphorylated

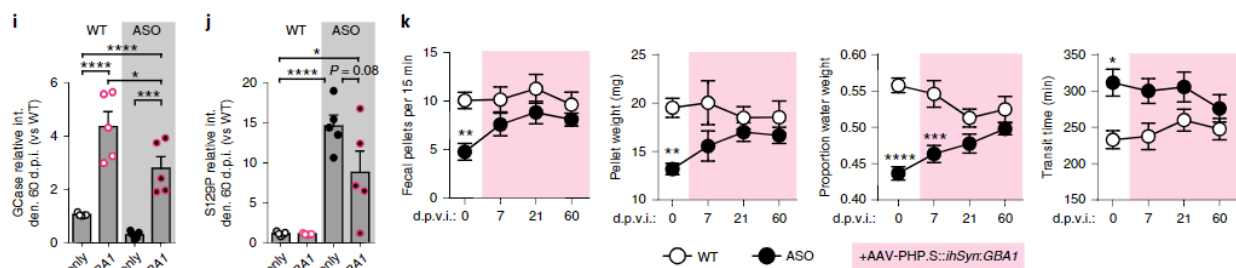


Figure 1.1. Glucocerebrosidase therapy reduces phosphorylated alpha synuclein and improves gut transit times in the ASO model of PD.

Content from: Challis C, Hori A, Sampson TR, Yoo BB, Challis RC, Hamilton AM, Mazmanian SK, Volpicelli-Daley LA, Gradinaru V. Gut-seeded α -synuclein fibrils promote gut dysfunction and brain pathology specifically in aged mice. *Nature Neuroscience*. 2020 Mar;23(3):327-336. doi: 10.1038/s41593-020-0589-7.

alpha synuclein and improve gut transit times in a mouse model of PD (Figure 1.1). Deep mechanistic understanding of biochemical pathways enabled the link between these two very different disorders to be exploited for therapeutic purposes.

PRECISION IN GENE THERAPY DELIVERY CAN ENABLE EFFICACIOUS, CURATIVE BENEFITS WHILE MINIMIZING OFF-TARGET, DANGEROUS SIDE EFFECTS

Gene therapy development has demonstrated the grand potential for successful clinical outcomes, but has also uncovered safety challenges that require further honing of technology. Precision in gene delivery can minimize some of the most severe acute problems that have arisen for patients in clinical trials. Utilization of AAVs instead of Adenovirus, for example, is an advancement in safety that has improved patient outcomes by decreasing adverse events (Marshall 1999). However, adverse events are still common with AAV trials, especially for indications related to the CNS, and using naturally occurring AAV serotypes (Duan 2023, Shen 2022).

Systemically delivered AAVs can noninvasively target therapeutic genetic cargo to diverse disease loci, but at high doses required for therapeutic penetrance, these vectors can cause severe toxicity, emphasizing the need for targeted, efficient gene delivery vectors (Duan 2023). Improved targeting of AAVs as developed by the Gradinaru Lab and other entities may further improve safety by limiting off-target transduction of tissues that are not relevant to disease processes affecting patient outcomes, and are being used to achieve targeted expression in both preclinical and non-clinical applications (Table 1.1; Challis 2022). These tissues, particularly the liver, are responsible for much of the acute burden of adverse events in the clinical trials population across therapies for multiple organ systems. Poor targeting also contributes to massive cost, as the dosages required for efficacy may be wasted across cells that are more responsible for severe side effects than therapeutic benefit.

CHALLENGES OF GENE THERAPY CARGO EXPRESSION DEMONSTRATE A NEED FOR CAREFUL THERAPEUTIC MOTIF DESIGN CHOICES

While delivery targeting would most immediately impact short term safety, cargo engineering can enable tighter transgene expression control and improve the long-term safety profiles of these

therapies (Table 1.1). For example, while Zolgensma, the latest success story in gene therapy, has shown curative outcomes in human children for a handful of years, overexpression toxicity in animal models including primate studies, forewarns of degeneration in later years (Hinderer 2018, Van Alstyne 2021). This effect appears not to be limited to SMN1, but rather, to be a broadly inducible phenomenon after ectopic expression of therapeutically relevant transgenes. In Rett Syndrome (RTT), the dosage sensitive gene methyl-CpG Binding Protein 2 (MECP2) is deficient, either in expression or activity, depending on the specific mutation incurred. Loss of even 30% of protein activity can cause mild forms of RTT, with severity increasing in a dose-dependent manner (Matagne 2021). Interestingly, overexpression of the MeCP2 protein by so much as two-fold induces a different neurodevelopmental disorder called MeCP2 Duplication Syndrome, characterized by neurologic and motor phenotypes similar to Rett Syndrome. In model animals, introduction of ectopic MeCP2 using gene therapy approaches has been shown to induce changes in neuronal morphology and connectivity, and even early death of the animal from overexpression toxicity, as separately defined from viral vector-associated toxicity (Gadalla 2017, Chao 2007).

Even genes not clinically associated with a need for tightly controlled expression have shown toxic overexpression phenotypes when expressed at levels higher than what is typically seen in healthy physiology. One example is frataxin (FXN), a gene which when under expressed, causes Friedreich's Ataxia, a neurodegenerative disorder of childhood. This gene encodes the frataxin protein (Fxn), which enhances mitochondrial robustness to oxidative damage through sequestering free iron and sulfur in the cell (Gonzalez-Cabo 2013). Efforts to replace FXN expression through gene therapy in animal models have shown phenotypic rescue in multiple organ systems, lending credence to the feasibility of human gene therapy's successful development. However, close study of these model animals over time reveals that there are also limits to its tolerability, and those limits are specific to local tissue environment. For example, Belbellaa et al. found that the threshold for toxicity in the heart occurs between 9-20 times the endogenous expression level in the heart, and that the mechanism for this toxicity was directly involving the resultant imbalance caused by more abundant Fxn carrying out its native function, but at a level that perturbed the general homeostasis of mitochondria (Belbellaa 2020). As the cell is highly complex, with many processes sharing raw

materials and byproducts in parallel, it is prudent to consider ways to control expression level of any ectopic gene, lest the therapeutic effect tips a cell or organ into a different dysfunctional state.

Table 1.1. A Selection of Preclinical and Clinical Progress in Developing AAV-based Gene Therapies for Disorders Affecting the Nervous System. Challenges, limitations, and progress exist in both the delivery and cargo technology spheres.

Translation Stage	Disease	Gene	Approach; Route of Administration	Challenges and Limitations	Progress and Emerging Solutions
Neurodevelopmental Disorders					
Preclinical	Neurofibromatosis Type 1	NF1	Augmentation, editing	Gene size (8.3 kb) is too large to package in existing capsids for replacement	Expanded capacity capsids, dual-vector approaches, cargo engineering of functional truncated therapeutic cargo, gene activation or gene editing approaches
Preclinical	Rett Syndrome	MeCP2	Replacement; intravenous	Dosage sensitivity, off-target toxicity (Matagne 2021) and overexpression toxicity	Inclusion of synthetic regulatory elements to regulate gene expression (Sinnott 2021)
Preclinical	CDKL5 deficiency	CDKL5	Replacement; intravenous	Penetrance of therapy at safe dosages of existing vectors	Boost efficacy by engineering therapeutic cassette to include secreted form of translated therapeutic protein (Medici 2021)
Lysosomal Storage Disorders					
Clinical	Mucopolysaccharidosis Type II	hIDS	Editing (ZFN-mediated replacement); intravenous	Efficacy of therapy at tolerated dosage (Sheridan 2018)	High efficiency capsids and promoters
Clinical	Tay Sachs	HexA/B	Replacement; intrathecal	Durability of Treatment (Flotte 2022)	Capsid serotypes that can achieve safety and efficacy with multiple administrations
Preclinical	Niemann-Pick Disease	NPC1	Replacement; intravenous	Penetrance and efficiency of therapy at tolerable dosages	Increased efficiency and efficacy with brain tropic vectors (Davidson 2021)
Ophthalmologic Disorders					
Clinical	Retinitis Pigmentosa	RPE65	Replacement; intravitreal	Poor diffusion of AAV within intravitreal space. Approach only applicable to known genetic cause	AAV capsid engineering for stability and improved diffusion in target environment (Dalkara 2013)

Clinical	Blindness (broad)	Cone Opsin	Substitution; intravitreal	Causes of blindness may be multifactorial, making genetic target identification difficult	Use cargo that is agnostic to the cause of pathology (Ratner 2021)
Clinical	Lebers Congenital Amaurosis type 2	CEP290	Editing; intravitreal	Gene size is too large to package in existing vectors	Editing to remove splice donor caused by disease mutation (Editas Medicine 2021)
Neurodegenerative Disorders					
Clinical	Parkinson's Disease	GAD, GDNF, NTN, AADC	Supplementation; intraparenchymal (putamen)	Invasive procedure targeting small cell population, complex genetic etiology for target gene identification	Targeted vectors with controlled systemic delivery methods (FUS) (Hsu 2013, Weber-Adrian 2021), cargo design enabling dopamine-augmentation via supplementation of growth factors or enzymes, agnostic to root-cause of pathology (McFarthing 2019)
Clinical	Huntington's Disease	HTT	RNA interference; intraparenchymal (striatum) (Rodrigues 2020)	General ectopic RNA overexpression toxicity (Grimm 2006)	Promoter and regulatory elements to mitigate cargo toxicity (Aguiar 2017)
Clinical	Alzheimer's disease	BDNF, hNGF, hTERT	Supplementation; intraparenchymal	Invasive procedure targeting small cell population with poor parenchymal spread (Castle 2020), complex genetic etiology	MRI-guided direct injections, increase cell specificity of systemic AAVs, cargo design for supplementation of neuroprotective factors
Preclinical	Alzheimer's disease	MAPT	Editing (ZFN); intraparenchymal and intravenous	Complex genetic etiology for target gene identification	Choice of target at the level of the observed pathology: ZFN mediated knockdown to reduce tau aggregates (Wegmann 2021)
Preclinical	Familial Alzheimer's Disease	APP ^{swe}	Editing; intravenous	Treatment approach is specific to mutation and may not be broadly applicable to entire disease population, requires high precision for efficacy.	Targeted editing of mutated APP allele (Duan 2022)
Neuromuscular Disorders					

Clinical and Preclinical	Spinal Muscular Atrophy	SMA1	Replacement; intrathecal, intravenous	Overexpression toxicity, inflammation and tissue pathology (Hordeaux 2020), safety concern for increased dosages required for older children with SMA2/3	Targeted delivery vectors to increase efficiency, regulated gene expression (Hordeaux 2020)
Clinical	Duchenne Muscular Dystrophy	DMD	Augmentation, Replacement; intramuscular, intravenous	Native gene size exceeds packaging capacity, tolerability of high vector dosages required for efficacy	Miniaturized therapeutic cassette (Philippidis 2022), nucleotide driven therapeutic strategy to correct exon skipping in patient subset (Dhillon 2020), targeted delivery vectors
Clinical	X-linked Myotubular Myopathy	MTM1	Replacement; intravenous	Acute liver failure at high therapeutic dosages (AAV8) in children with pre-existing liver dysfunction	Targeted delivery vectors, clinical support/immunosuppression
Disorders affecting the Peripheral Nervous System					
Clinical	Transthyretin amyloidosis with polyneuropathy	TTR	Editing; intravenous	While effective, existing therapies (tafamidis, patisiran, inotersin) require lifelong drug therapy with notable side effects, and do not completely prevent disease progression	Single dose AAV enables lasting correction (Gillmore 2021)
Other Non-Genetic and Multifactorial Neurological and Ophthalmologic Disease					
Preclinical	Stroke, Tumor, Traumatic Brain Injury	Wnt7a/b	Supplementation; intravenous	Multifactorial, non-genetic causes require treatment that is agnostic to a specific gene or mutation	Generally enhance BBB endothelial cell health through developmental regulation, without regard to the nature of the specific insult causing disease (Martin 2022)
Preclinical	Chronic Pain	Nav1.7	Editing; intrathecal	Multifactorial, non-genetic causes require treatment that is agnostic to a specific gene or mutation	Decreasing pain sensation propagation to the brain by specifically decreasing expression of a sodium channel involved with pain propagation (Moreno 2021)

EXPLOITING THE MODULARITY AND PRECISION OF GENE THERAPY CARGO COMPONENTS TO SPEED THE PARALLEL DEVELOPMENT OF SAFER GENE THERAPIES FOR DISORDERS WITH SHARED PATHOPHYSIOLOGIC ATTRIBUTES

The inherent modularity of gene therapy exceeds the scope of other pharmaceutical products. Genetic medicines have the potential be designed to work dynamically and exert their effects only where, when, at what level and in response to which stimuli the developer chooses. Innovation in this area, and exploration of different approaches to restore healthy balances of therapeutic components within cells' disease environments, will expand their benefit and utility. The work herein describes my efforts to advance these capabilities with the following approaches that can be implemented across genetic disorders that share common properties without regard to how they are traditionally classified by organ system as human diseases:

1. Mimicking healthy patterns of transgene expression through incorporation of native gene regulatory elements.
2. Delivery-agnostic expression regulation to circumvent overexpression toxicity.
3. AAV-genome-specific silencing to reverse deleterious effects observed after AAV administration.

CHAPTER 1 REFERENCES

Lander, E.S., Linton, L.M., Birren, B., Nusbaum, C., Zody, M.C., Baldwin, J., Devon, K., Dewar, K., Doyle, M., FitzHugh, W., et al. (2001). Initial sequencing and analysis of the human genome. *Nature* 409, 860–921.

Amberger, J.S., Bocchini, C.A., Schiettecatte, F., Scott, A.F., and Hamosh, A. (2015). OMIM.org: Online Mendelian Inheritance in Man (OMIM®), an online catalog of human genes and genetic disorders. *Nucleic Acids Res.* 43, D789–D798.

Max Roser, Hannah Ritchie and Fiona Spooner (2021) - “Burden of Disease” Published online at OurWorldInData.org. Retrieved from: '<https://ourworldindata.org/burden-of-disease>' [Online Resource]

Klimova, B., Storek, M., Valis, M., and Kuca, K. (2017). Global View on Rare Diseases: A Mini Review. *Curr. Med. Chem.* 24, 3153–3158.

Challis C, Hori A, Sampson TR, Yoo BB, Challis RC, Hamilton AM, Mazmanian SK, Volpicelli-Daley LA, Gradinaru V. Gut-seeded α -synuclein fibrils promote gut dysfunction and brain pathology specifically in aged mice. *Nature Neuroscience*. 2020 Mar;23(3):327-336. doi: 10.1038/s41593-020-0589-7.

Marshall, E. (1999). Gene therapy death prompts review of adenovirus vector. *Science* 286, 2244–2245.

Duan, D. (2023). Lethal immunotoxicity in high-dose systemic AAV therapy. *Mol. Ther.* 31, 3123–3126.

Shen, W., Liu, S., and Ou, L. (2022). rAAV immunogenicity, toxicity, and durability in 255 clinical trials: A meta-analysis. *Front. Immunol.* 13, 1001263.

Challis, R.C., Ravindra Kumar, S., Chen, X., Goertsen, D., Coughlin, G.M., Hori, A.M., Chuapoco, M.R., Otis, T.S., Miles, T.F., and Gradinaru, V. (2022). Adeno-Associated Virus Toolkit to Target Diverse Brain Cells. *Annu. Rev. Neurosci.* 45, 447–469.

Van Alstyne, M., Tattoli, I., Delestrée, N., Recinos, Y., Workman, E., Shihabuddin, L.S., Zhang, C., Mentis, G.Z., and Pellizzoni, L. (2021). Gain of toxic function by long-term AAV9-mediated SMN overexpression in the sensorimotor circuit. *Nat. Neurosci.* 24, 930–940.

Hinderer, C., Katz, N., Buza, E.L., Dyer, C., Goode, T., Bell, P., Richman, L.K., and Wilson, J.M. (2018). Severe Toxicity in Nonhuman Primates and Piglets Following High-Dose Intravenous Administration of an Adeno-Associated Virus Vector Expressing Human SMN. *Hum. Gene Ther.* 29, 285–298.

Gadalla, K.K.E., Vudhironarit, T., Hector, R.D., Sinnett, S., Bahey, N.G., Bailey, M.E.S., Gray, S.J., and Cobb, S.R. (2017). Development of a Novel AAV Gene Therapy Cassette with Improved Safety Features and Efficacy in a Mouse Model of Rett Syndrome. *Mol Ther Methods Clin Dev* 5, 180–190.

Matagne, V., Borloz, E., Ehinger, Y., Saidi, L., Villard, L., and Roux, J.-C. (2021). Severe offtarget effects following intravenous delivery of AAV9-MECP2 in a female mouse model of Rett syndrome. *Neurobiol. Dis.* 149, 105235.

Chao, H.-T., Zoghbi, H.Y., and Rosenmund, C. (2007). MeCP2 controls excitatory synaptic strength by regulating glutamatergic synapse number. *Neuron* 56, 58–65.

Belbellaa, B., Reutenauer, L., Messaddeq, N., Monassier, L., and Puccio, H. (2020). High Levels of Frataxin Overexpression Lead to Mitochondrial and Cardiac Toxicity in Mouse Models. *Mol Ther Methods Clin Dev* 19, 120–138.

Sheridan, C. (2018). Sangamo's landmark genome editing trial gets mixed reception. *Nat. Biotechnol.* 36, 907–908.

Medici, G., Tassinari, M., Galvani, G., Bastianini, S., Gennaccaro, L., Loi, M., Mottolese, N., Alvente, S., Berteotti, C., Sagona, G., et al. (2021). Expression of a secretable, cell-penetrating cdk15 protein enhances the efficacy of aav vector-mediated gene therapy for cdk15 deficiency disorder. *bioRxiv*. 10.1101/2021.07.26.453746.

Matagne, V., Borloz, E., Ehinger, Y., Saidi, L., Villard, L., and Roux, J.-C. (2021). Severe offtarget effects following intravenous delivery of AAV9-MECP2 in a female mouse model of Rett syndrome. *Neurobiol. Dis.* 149, 105235.

Dalkara, D., Byrne, L.C., Klimczak, R.R., Visel, M., Yin, L., Merigan, W.H., Flannery, J.G., and Schaffer, D.V. (2013). In vivo-directed evolution of a new adeno-associated virus for therapeutic outer retinal gene delivery from the vitreous. *Sci. Transl. Med.* 5, 189ra76.

Davidson, C.D., Gibson, A.L., Gu, T., Baxter, L.L., Deverman, B.E., Beadle, K., Incao, A.A., Rodriguez-Gil, J.L., Fujiwara, H., Jiang, X., et al. (2021). Improved systemic AAV gene therapy with a neurotrophic capsid in Niemann-Pick disease type C1 mice. *Life Sci Alliance* 4. 10.26508/lsa.202101040.

Flotte, T.R., Cataltepe, O., Puri, A., Batista, A.R., Moser, R., McKenna-Yasek, D., Douthwright, C., Gernoux, G., Blackwood, M., Mueller, C., et al. (2022). AAV gene therapy for Tay-Sachs disease. *Nat. Med.* 28, 251–259.

Ratner, M. (2021). Light-activated genetic therapy to treat blindness enters clinic. *Nat. Biotechnol.* 39, 126–127.

“Editas Medicine Announces Positive Initial Clinical Data from Ongoing Phase 1/2 Brilliance Clinical Trial of Edit-101 for LCA10.” Editas Medicine, 29 Sept. 2021, ir.editasmedicine.com/news-releases/news-release-details/editas-medicine-announces-positive-initial-clinical-data-ongoing.

Hsu, P.-H., Wei, K.-C., Huang, C.-Y., Wen, C.-J., Yen, T.-C., Liu, C.-L., Lin, Y.-T., Chen, J.-C., Shen, C.-R., and Liu, H.-L. (2013). Noninvasive and targeted gene delivery into the brain using microbubble-facilitated focused ultrasound. *PLoS One* 8, e57682.

Moreno, A.M., Alemán, F., Catroli, G.F., Hunt, M., Hu, M., Dailamy, A., Pla, A., Woller, S.A., Palmer, N., Parekh, U., et al. (2021). Long-lasting analgesia via targeted in situ repression of NaV1.7 in mice. *Sci. Transl. Med.* 13. [10.1126/scitranslmed.aay9056](https://doi.org/10.1126/scitranslmed.aay9056).

Martin, M., Vermeiren, S., Bostaille, N., Eubelen, M., Spitzer, D., Vermeersch, M., Profaci, C.P., Pozuelo, E., Toussay, X., Raman-Nair, J., et al. (2022). Engineered Wnt ligands enable blood-brain barrier repair in neurological disorders. *Science* 375, eabm4459.

Gillmore Julian D., Gane Ed, Taubel Jorg, Kao Justin, Fontana Marianna, Maitland Michael L., Seitzer Jessica, O’Connell Daniel, Walsh Kathryn R., Wood Kristy, et al. (2021). CRISPR-Cas9 In Vivo Gene Editing for Transthyretin Amyloidosis. *N. Engl. J. Med.* 385, 493–502.

Dhillon, S. (2020). Viltolarsen: First Approval. *Drugs* 80, 1027–1031.

Philippidis, A. (2022). After Patient Death, FDA Places Hold on Pfizer Duchenne Muscular Dystrophy Gene Therapy Trial. *Hum. Gene Ther.* 33, 111–115.

Hordeaux, J., Buza, E.L., Dyer, C., Goode, T., Mitchell, T.W., Richman, L., Denton, N., Hinderer,

C., Katz, N., Schmid, R., et al. (2020). Adeno-Associated Virus-Induced Dorsal Root Ganglion Pathology. *Hum. Gene Ther.* 31, 808–818.

Hordeaux, J., Buza, E.L., Jeffrey, B., Song, C., Jahan, T., Yuan, Y., Zhu, Y., Bell, P., Li, M., Chichester, J.A., et al. (2020). MicroRNA-mediated inhibition of transgene expression reduces dorsal root ganglion toxicity by AAV vectors in primates. *Sci. Transl. Med.* 12. 10.1126/scitranslmed.aba9188.

Duan, Y., Ye, T., Qu, Z., Chen, Y., Miranda, A., Zhou, X., Lok, K.-C., Chen, Y., Fu, A.K.Y., Gradinaru, V., et al. (2022). Brain-wide Cas9-mediated cleavage of a gene causing familial Alzheimer's disease alleviates amyloid-related pathologies in mice. *Nat Biomed Eng* 6, 168–180.

Wegmann, S., DeVos, S.L., Zeitler, B., Marlen, K., Bennett, R.E., Perez-Rando, M., MacKenzie, D., Yu, Q., Commins, C., Bannon, R.N., et al. (2021). Persistent repression of tau in the brain using engineered zinc finger protein transcription factors. *Sci Adv* 7. 10.1126/sciadv.abe1611.

Castle, M.J., Baltanás, F.C., Kovacs, I., Nagahara, A.H., Barba, D., and Tuszynski, M.H. (2020). Postmortem Analysis in a Clinical Trial of AAV2-NGF Gene Therapy for Alzheimer's Disease Identifies a Need for Improved Vector Delivery. *Hum. Gene Ther.* 31, 415–422.

Aguiar, S., van der Gaag, B., and Cortese, F.A.B. (2017). RNAi mechanisms in Huntington's disease therapy: siRNA versus shRNA. *Transl. Neurodegener.* 6, 30.

Rodrigues, F.B., and Wild, E.J. (2020). Huntington's Disease Clinical Trials Corner: April 2020. *J. Huntingtons Dis.* 9, 185–197.

Grimm, D., Streetz, K.L., Jopling, C.L., Storm, T.A., Pandey, K., Davis, C.R., Marion, P., Salazar, F., and Kay, M.A. (2006). Fatality in mice due to oversaturation of cellular microRNA/short hairpin RNA pathways. *Nature* 441, 537–541.

McFarthing, K., Prakash, N., and Simuni, T. (2019). CLINICAL TRIAL HIGHLIGHTS: 1. GENE THERAPY FOR PARKINSON'S, 2. PHASE 3 STUDY IN FOCUS - INTEC PHARMA'S ACCORDION PILL, 3. CLINICAL TRIALS RESOURCES. *J. Parkinsons. Dis.* 9, 251–264.

Weber-Adrian, D., Kofoed, R.H., Silburt, J., Noroozian, Z., Shah, K., Burgess, A., Rideout, S., Kügler, S., Hynynen, K., and Aubert, I. (2021). Systemic AAV6-synapsin-GFP administration results in lower liver biodistribution, compared to AAV1&2 and AAV9, with neuronal expression following ultrasound-mediated brain delivery. *Sci. Rep.* 11, 1934.

Chapter 2

MIMICKING HEALTHY PATTERNS OF ENDOGENOUS EXPRESSION THROUGH IDENTIFICATION AND INCORPORATION OF NATIVE REGULATORY ELEMENTS

This chapter contains work described in the following prior abstracts and presentations, and is in preparation for submission at *Neuron*:

Hori AM, Grebin A, Robinson JE, Chen X, Flytzanis N, Goeden N, Chan K, Deverman B, Gradinaru V. Targeted Gene Therapy with Engineered Systemic AAVs for the Central and Peripheral Nervous Systems Prevents Motor Coordination Phenotypes in a Mouse Model of Friedreich's Ataxia. ASGCT Annual Meeting Abstracts, Molecular Therapy, Volume 29, Issue 4, Supplement 1, 2021, Pages 1-427, ISSN 1525-0016, <https://doi.org/10.1016/j.ymthe.2021.04.019>.

Hori AM, Robinson JE, Chan K, Flytzanis N, Goeden N, Deverman B, Gradinaru V. Recombinant AAVs Target Custom Frataxin Therapeutic Cassettes to Tissues of Pathophysiologic Relevance in Friedreich's Ataxia. 2020 ASGCT Annual Meeting Abstracts, Molecular Therapy, Volume 28, Issue 4, Supplement 1, 2020, Pages 1-592, ISSN 1525-0016, <https://doi.org/10.1016/j.ymthe.2020.04.019>.

ABSTRACT

In Friedreich's Ataxia (FA), insufficient expression of frataxin (FXN) increases susceptibility to oxidative stress in multiple organ systems. Neuronal degeneration in the central and peripheral nervous systems cause loss of motor coordination, while cardiomyopathy contributes to early death. In this study, AAV.CAP-B10 and AAV-PHP.PNS2, two CNS and PNS directed AAV capsids were used individually and in conjunction to replace FXN across sites of pathophysiologic relevance, while detargeting the liver and cell types typically spared in human disease. A therapeutic construct containing FXN and its putative gene regulatory elements was packaged into AAVs and systemically administered to inducible shRNA-based FXN knockdown mice prior to doxycycline-induction of the disease phenotype. Motor, sensory and cardiac function were assessed before quantitative tissue analysis was performed to assess FXN levels and pathologic hallmarks. Ectopic FXN expression mimicked endogenous patterns of non-diseased mice in target tissues, with reduced liver expression. When delivered in combination, pan-nervous system AAV-FXN prevented induction of motor and coordination deficits compared to controls. However, delivery to either the CNS or PNS alone failed

to provide this benefit. These findings demonstrate the utility of engineered AAVs for probing questions of tropism in precision gene therapy applications for neurodegenerative disease.

INTRODUCTION

Friedreich's Ataxia (FA) is a neurodegenerative disease in which an intronic triplet repeat expansion mutation causes insufficient production of a protein called frataxin (FXN) (Campuzano 1996, Koeppen 2011). Without enough frataxin, mitochondrial iron-sulfur clustering becomes dysfunctional, leaving cells vulnerable to reactive oxygen species. Cellular damage is pathological to tissues with intense energetic needs and low capacity for regeneration, such as the brain, peripheral nerves and heart. Resultant deficiencies in balance, movement coordination, and heart function lead to loss of body control (ataxia) and early death (Koeppen 2011, Gonzalez-Cabo 2013).

Because FA is well described as a genetic disorder stemming from loss of expression of the gene of interest, it follows, and a few groups have hypothesized, that simple gene replacement should be able to mitigate, if not reverse, FA pathology. Indeed, it has been shown that restoring a normal copy of *FXN* in some murine models leads to increased levels of frataxin protein expressed in the brain or body (Perdomini 2014, Piguet 2018). It has also been observed that the limit of tolerability to ectopic FXN is between 9- to 20-fold the endogenous level; overexpression achieved using the CAG promoter to drive FXN expression, delivered by AAV9 at clinically relevant dosages, was sufficient to cause cardiotoxicity and liver regeneration to replace damaged cells in the Myc-Cre model (Belbellaa 2020, Huichalaf 2022).

One problem with gene therapy for diseases involving the brain is efficient, brain-wide delivery that minimizes invasiveness, within the limits of therapeutic administration dosages (Zlokovic 1997). To address this, we employ engineered AAV viruses that, when administered systemically, can deliver genes of interest to target cells across the blood-brain-barrier. In addition to delivering and expressing genetic cargo in the brain, these systemic viruses exhibit preferential transduction in different peripheral organs and cell types, offering enhanced capability for targeted gene delivery to

address multi-organ pathologies (Chan 2017, Kumar 2020). In addition to increasing transduction efficiency at clinically relevant sites, cell tropism patterns of these vectors avoid off-target transduction of organs and cell types commonly associated with AAV-associated complications across species, including in human gene therapy clinical trials (Goertsen 2022, Challis 2022).

In this study, we deliver FXN therapeutic cargo to tissues of interest in a mouse model of FA through combined administration of two next-generation AAVs: AAV-CAP.B10 and AAV-PHP.PNS2 (Goertsen 2022). We observe that the top therapeutic gene construct we created expresses FXN in the same brain regions where it is highly expressed in non-diseased, wildtype mice, and where it has been observed to be deficient in patients with Friedreich's Ataxia from postmortem analysis. In addition, we observe construct expression in another key therapeutic target in FA, the dorsal root ganglia (DRGs). These findings demonstrate a multimodal approach combining delivery methods with cargo design to achieve recapitulation of healthy therapeutic transgene expression patterns.

MIMICKING HEALTHY PATTERNS OF ENDOGENOUS EXPRESSION THROUGH IDENTIFICATION AND INCORPORATION OF NATIVE REGULATORY ELEMENTS FOR FRIEDREICH'S ATAXIA GENE THERAPY

We designed and generated three AAV-FXN expression vectors. In the first, the FXN gene is expressed as a cDNA from the strong, ubiquitous CAG promoter (CAG-FXN). We expected this promoter to express FXN in most cell types within and outside the CNS. The use of a strong promoter may not be optimal, given that endogenous FXN is expressed at relatively low levels (Evans-Galea

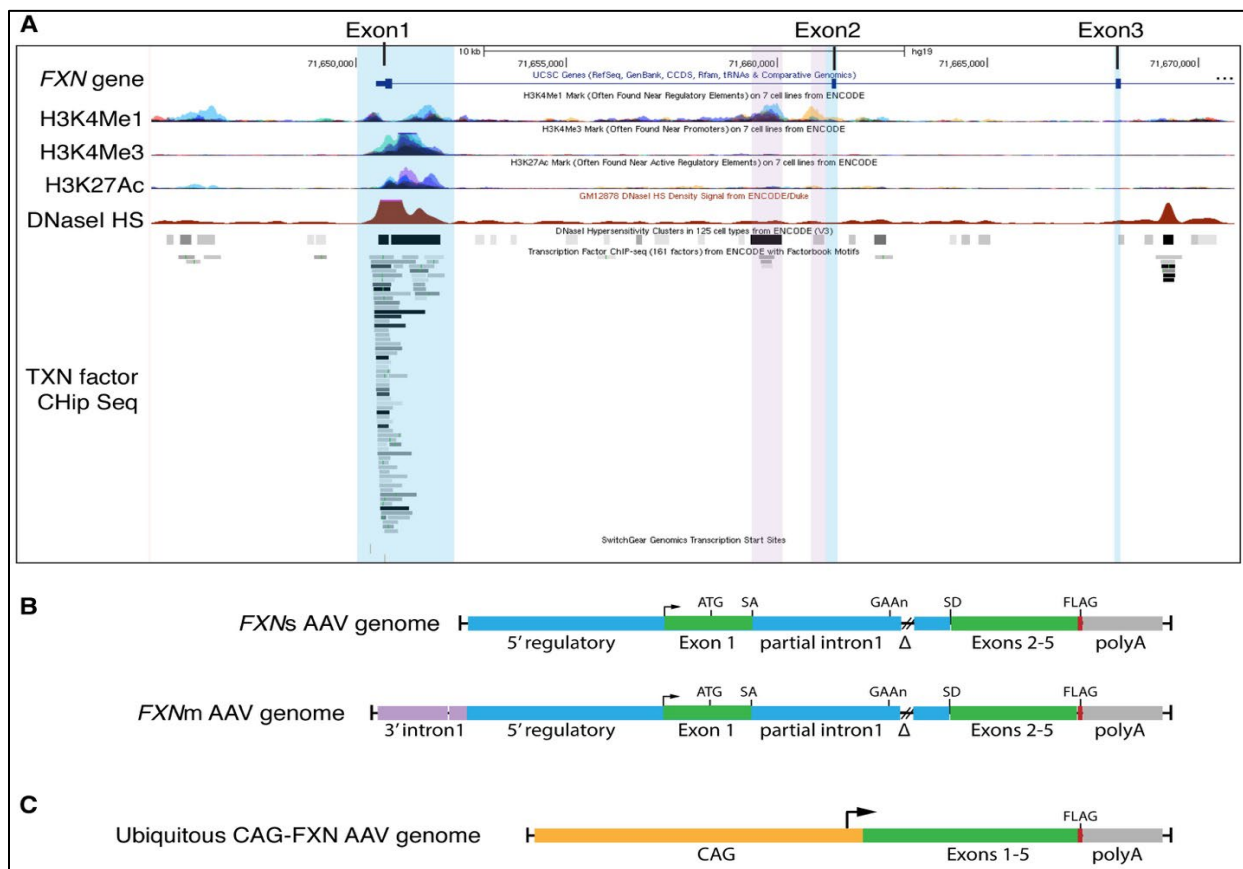


Figure 2.1. Incorporating the predicted human FXN gene regulatory elements into AAV genomes. (A) Encode data from the UCSC genome browser shows H3K4Me1 (putative regulatory elements), H3K4Me3 (putative promoter), H3K27Ac (putative active promoter) marks, and DNaseI hypersensitivity sites. Regions highlighted in light blue are used in both *FXN* vectors. Potential enhancer elements highlighted in purple are present exclusively in the AAV-*FXNm* vector. (B) Schematics of the *FXN* gene AAV genomes. Blue and light purple regions correspond to genomic regions shown in A. *FXN* coding regions are shown in green and the Flag tag is shown in red. (C) Schematic of the CAG-*FXN* AAV genome.

2014). To express FXN at levels that correspond more closely to endogenous FXN expression, we developed AAV vectors that carry a truncated human FXN gene, along with a candidate putative native promoter and putative gene regulatory elements (Figure 2.1). We identified putative core promoter and enhancer sequences that regulate FXN expression using the UCSC genome browser and Encode data <http://genome.ucsc.edu/>. DNaseI hypersensitivity, methylation and acetylation marks suggest the location of the core promoter within a ~2300 bp region that includes sequences 5' to the transcriptional start site, exon 1 and part of intron 1 (Fig 2.1A). In addition, H3K4Me1 and DNase hypersensitivity sites suggest that additional enhancer sequences may be present within intron 1 closer to the intron 1 – exon 2 boundary. Based on this analysis, we generated two AAVFXN gene vectors: AAV-FXNs and AAV-FXNm. AAV-FXNs comprises the ~2300 bp putative FXN core promoter, the intron 1 splice acceptor sequences and a fusion of exons 2-5 (Fig. 2.1B). AAV-FXNm has the sequence in AAV-FXNs plus two additional potential enhancer sites. These elements have been added 5' of the core promoter region of AAV-FXNs to create AAV-FXNm. All three constructs use a polyA signal from the *GHI* gene and are tagged at the 3' end of the FXN coding sequences with a FLAG epitope for immunohistochemistry.

After sequence confirmation, we evaluated these vectors for FXN expression in cell culture. We generated the three AAV-FXN viruses, and then used the AAVs to transduce HEK293 cells. Immunostaining for the FLAG tag demonstrated that all three viruses expressed ectopic FXN.

Engineered AAV capsids exhibit properties which enable differential transduction of distinct

tissues and cell types. In these experiments, we pair a CNS transducing AAV variant with a PNS transducing variant for a dual-vector delivery approach. Initial experiments were conducted using AAV-PHP.eB due to its ability to cross the blood brain barrier and broadly transduce cells in the CNS, while later experiments that were conducted in the inducible FXN knockdown model were

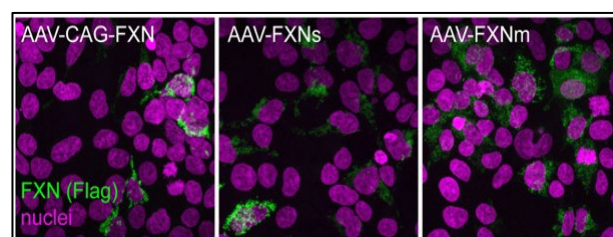


Figure 2.2. All three AAV-PHP.SN:FXN vectors express FXN in cell culture. FLAG IF (green) along with DAPI (magenta) in HEK293 cells transduced by AAV-PHP.SN viruses carrying the CAG-FXN (left), FXNs (middle) or FXNm (right) genome.

conducted using AAV-CAP-B.10 and AAV-PHP-PNS.2. Developed using the CREATE method, AAV-CAP-B.10 is a next generation variant of PHP.eB. It maintains PHP.eB's ability to cross the blood-brain-barrier, while exhibiting superior liver detargeting as evidenced by transduction patterns when packaging NLS-GFP (Deverman 2016, Goertsen 2022). This is accomplished through maintaining the PHP.eB mutation on AAV9's 588 residue and adding an additional mutation on an interacting loop at residue 455. In addition, compared to PHP.eB, AAV-CAP-B.10 seems to preferentially target neurons over other brain cell types, such as astrocytes and oligodendrocytes. In the cerebellum, AAV-CAP-B.10 transduces granular cells with higher efficiency than Purkinje cells (Goertsen 2022). This is significant, because this variant's transduction pattern is both more consistent with transduction patterns of FXN we observed in previous experiments, in addition to published pathology reports showing that Purkinje cells appeared relatively unaffected in postmortem analysis of FA patient brain tissue (Koeppen 2011). Thus, after its development, we transitioned all phase 2 experiments to utilize AAV-CAP-B.10 as the delivery vehicle most suited for CNS targeting of our therapeutic FXN construct. Both phases of the project paired a CNS transducing variant with our engineered PNS transducing variant, PHP.S. In experiments combining PHP.eB with PHP.S, this combination is referred to as AAV-PHP.SN, and experiments utilizing AAV-CAP.B10 and PHP.S are referred to as AAV-B10S. Later experiments which utilize the peripheral targeting vector described by Chen et al. and Chuapoco et al., AAV-MacPNS2, are referred to as AAV-B10PNS2 when used in conjunction with each other. Where vectors are used individually, they are referred to by their individual names.

TARGETED DELIVERY OF CUSTOM FXN CASSETTE RECAPITULATES HEALTHY PATTERNS OF FXN EXPRESSION IN THE CNS AND DRGS OF ADULT MICE

To assess the expression profiles of the candidate constructs, we injected three young adult WT C57Bl/6J mice per group with a combination of AAV-PHP.SN (3E11 vg/mouse of AAV-PHP.eB and 5E11 vg/mouse AAV-PHP.S) expressing FXN from one of the three FXN expressing genomes. These doses of AAV-PHP.eB and AAV-PHP.S were chosen based on quantification of NLS-GFP expression from each of the two vectors injected separately in a prior work (Chan 2017). Four weeks

post administration, the mice were euthanized and perfused for analysis of FXN expression by IHC. Using Flag IHC, we assessed FXN expression in the CNS and DRG. As expected based on published reporter data with the CAG promoter, the AAV PHP.SN:CAG-FXN vector combination expressed FXN broadly throughout the forebrain, brain stem, cerebellum, and spinal cord (Fig. 2.3). Remarkably, we observed FXN expression from the AAV-PHP.SN:FXNs and AAV-PHP.SN:FXNm vectors in many of the cell populations/regions known to be sensitive to reduced

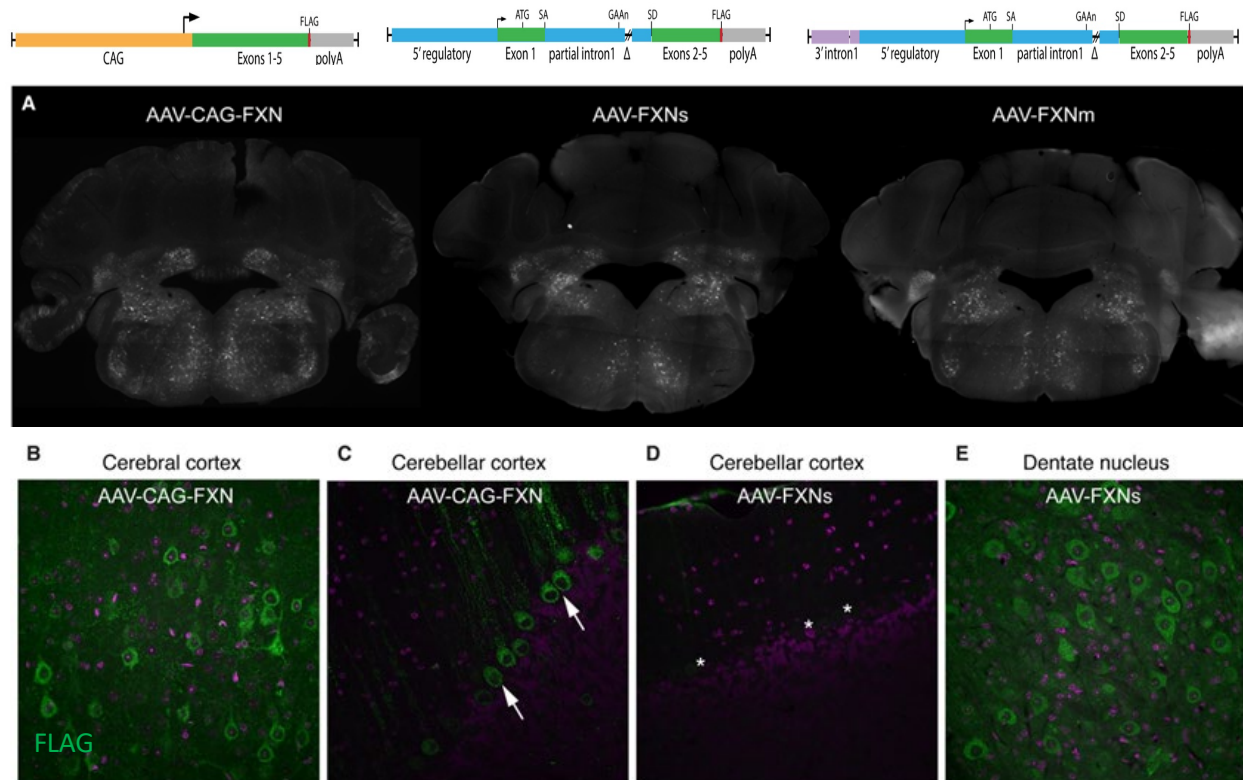


Figure 2.3. Comparison of expression patterns using ubiquitous or custom promoters and enhancers. A) Coronal slices of mouse brain transduced with the three candidate constructs delivered by AAV-PHP.eB, along with zoomed in images of FLAG staining in the cortex (B), cerebellum (C, D), and cerebellar dentate nucleus (E), illustrative of transduction pattern differences between the candidate constructs. The white arrows in (C) and asterisks in (D) indicate Purkinje cell bodies.

FXN expression in FA: DRGs, spinal cord, brain stem nuclei, and the deep cerebellar nuclei, including the dentate nucleus. FXN expression from the AAV-FXNs or AAV-FXNm vectors was comparatively weak in the forebrain (data not shown).

To further confirm that the vectors express FXN *in vivo* and compare it to endogenous FXN levels, we next used an anti-FXN antibody for IHC. In animals injected with the AAV-FXN vectors, this antibody gave strong staining in DRG and deep cerebellar nuclei that was consistent with the pattern of Flag staining (Fig. 2.4). Surprisingly, this antibody was more sensitive at detecting the AAV-delivered FXN than two different FLAG antibodies. With FXN IHC, we detected expression from all three vectors throughout the brain and spinal cord (Fig 2.4). Interestingly, the pattern of expression from the FXNs and FXNm vectors was distinct than that provided by the CAG-FXN vector in several ways. Expression from the FXNs and FXNm vectors was strongest in cells with neuronal morphology, while the expression from AAV-CAG-FXN was also observed in cells with the morphology of endothelial cells and astrocytes (Fig 2.4). Within the cerebellum, expression from the FXNm vector was strongest in the granule cell layer while the CAG promoter provided expression that was most notable in Purkinje cells (Fig. 2.4). In the striatum, the FXNm vector provided sparse expression. Staining in all areas was greatly elevated in mice that received AAV-FXN as compared to untreated controls. Nevertheless, the anti-FXN signal seen in untreated mice was present in all areas in which we saw AAV-FXNs or AAV-FXNm mediated FXN expression. This much weaker signal appeared to follow a similar pattern of expression, with a stronger signal notable in the dentate nucleus, substantia nigra (data not shown), medial septal nucleus and sparse cells in the striatum. Therefore, within the CNS, both AAV-FXNs and AAV-FXNm vectors provide a pattern of FXN expression that matches the pattern of FXN IHC in control mice (putative endogenous FXN expression) more closely than the CAG-FXN vector.

To further validate whether the differences in FXN expression levels we observed from the AAV-FXNs and AAV-FXNm vectors in the mouse match endogenous FXN expression in the human brain, we analyzed human transcriptome data available through the Allen Brain Atlas. These data suggest that FXN is more highly expressed in the dentate, cuneate, gracile and septal nuclei, substantia nigra, and other deep brain structures than in the cerebellar or cerebral cortices (Fig 2.5). Therefore, the human expression data further supports the use of the FXN gene regulatory elements to achieve FXN expression levels that better match endogenous FXN.

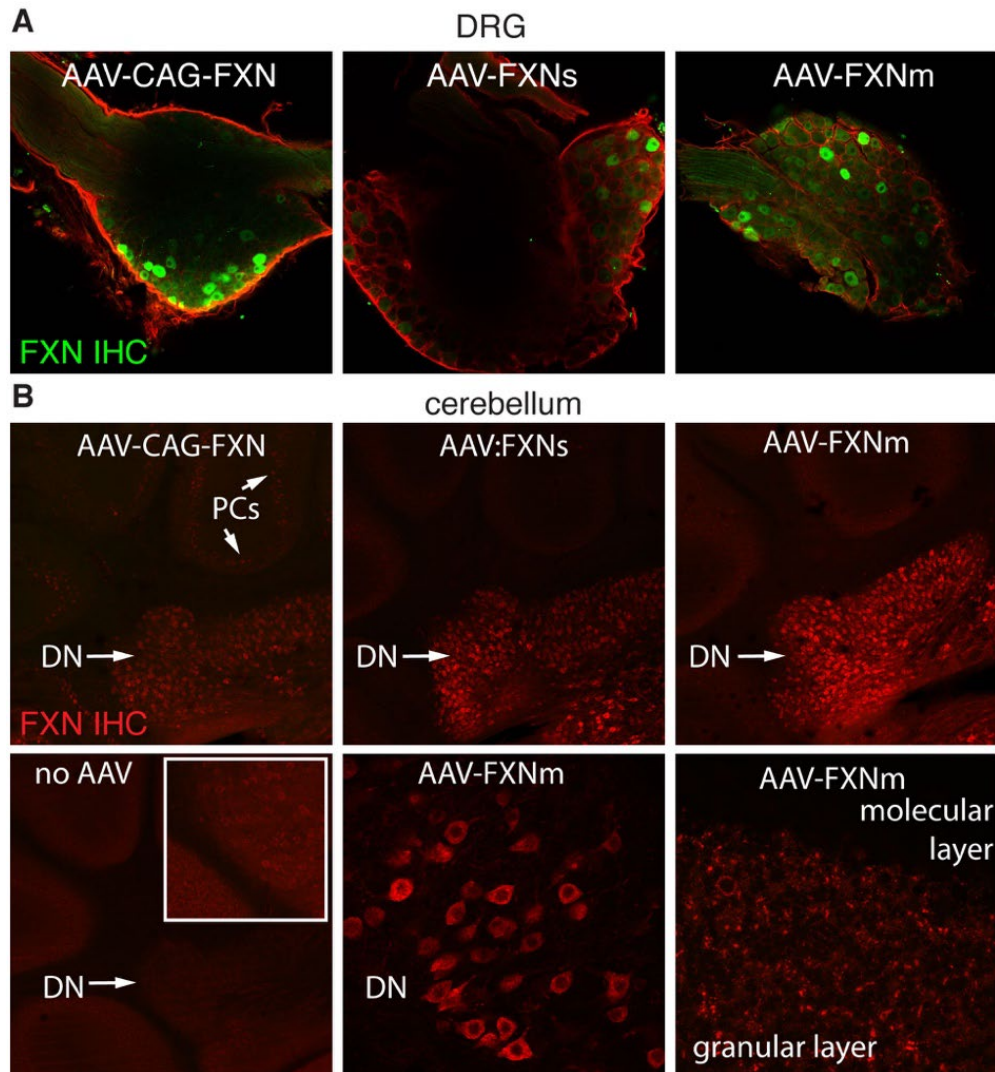


Figure 2.4. AAV-PHP.SN mediates expression in DRG and cerebellar nuclei following intravenous injection. Images show FXN IHC in the DRG (A, green) or cerebellum (B, red). All three vectors express FXN in the dentate nucleus (DN). Purkinje cell expression is notable from AAV-CAG-FXN (B, top left) but is weaker from FXNs or FXNm. Faint endogenous FXN is evident in the DN (bottom, left). 40X images of FXN IHC in the DN (bottom, middle) and granular layer of the cerebellum (bottom, right).

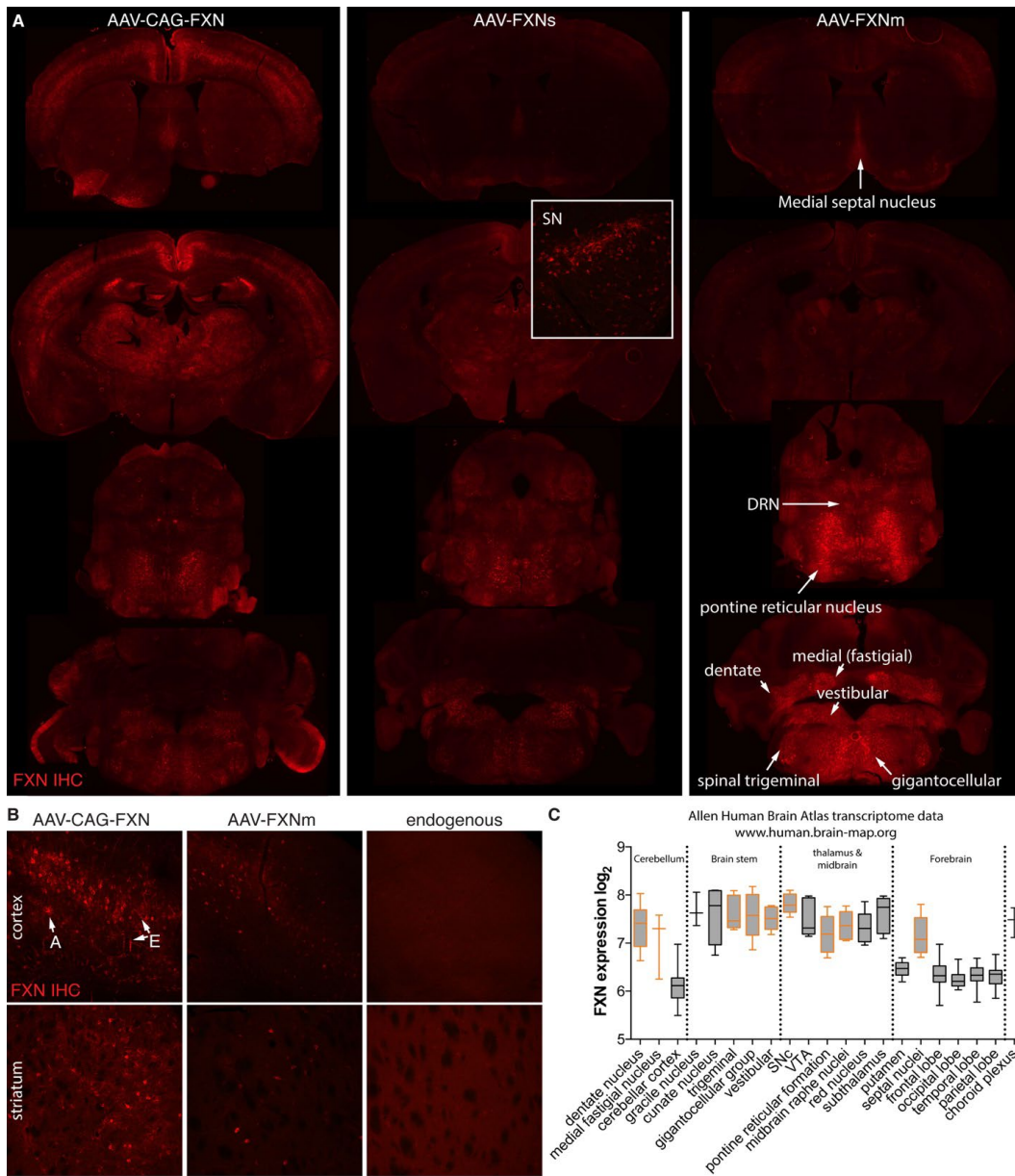


Figure 2.5. AAV-PHP.SN:FXNs and :FXNm vectors provide gene expression in the mouse brain that appears to correlate with endogenous mouse FXN expression and human brain transcriptome data. (A) FXN expression (red) from the indicated AAV-FXN vectors in brain sections displayed from rostral (top) to caudal (bottom). (B) Human FXN expression microarray data (probe A_23_P60517) from the Allen Brain Atlas (<http://human.brain-map.org>) suggests that FXN expression is higher in many deep brain nuclei relative to the cerebellar and cerebral cortices. The graph shows data from the indicated brain regions. Human microarray data highlighted in orange are matched to corresponding marked regions of the mouse brain sections with notable FXN expression (A). Substantia nigra, SN; dorsal raphe nucleus, DRN.

SELECTION OF MODEL MICE FOR ASSESSMENT OF EFFICACY

There are several lines of transgenic mice available that recapitulate important aspects of Friedreich's Ataxia. The most commonly used lines are Cre-recombinase dependent, and knock out endogenous expression of FXN in the cardiac or nervous system, depending upon the specific breeding strategy and experimental questions the researchers set out to answer. This strategy enables researchers to probe the effect of FXN replacement on organ system specific effects, such as utilizing the Myc-Cre mouse for studies on cardiac replacement of FXN. Each of these Cre-dependent models, while useful for targeted inquiry, fails to recapitulate the multisystem nature of the human disease, thus making it impossible to disentangle key synergies that may underlie the disease state or ability to intervene in classic disease manifestations.

For translational understanding, it is advantageous to use models that capture the system-wide effects of FXN depletion. We considered two models for our efficacy experiments: the knock-in knock-out model (KIKO), and the inducible knockdown model (FXNiKD). The KIKO model is a genetic recapitulation of the disorder. Knocking in a triplet repeat expansion into the FXN gene knocks out expression of FXN from the endogenous locus, and a neurologic phenotype has been described for these mice (McMackin 2017). However, despite being closest to the pathophysiologic cause of FA, this mouse model fails to show a cardiac deficit, which is the major cause of morbidity and mortality in human patients. The inducible model utilizes doxycycline to dose-dependently knock down expression of endogenous FXN through RNA interference, through expression of a small hairpin RNA from a doxycycline inducible promoter. After processing by the cell, the shRNA silences transcripts of the endogenous FXN, leading to low levels of Fxn protein (Chandran 2017). Though this model is more contrived in the way it achieves low levels of expression, it does exhibit both neurobehavioral and cardiac defects, like human patients. After design considerations ensuring our construct would not be knocked down by the shRNA in Chandran's model, we selected it for our testing so that we could test efficacy in a whole-body rodent model of FA.

DELIVERY OF HFXN TO TARGET CELL POPULATIONS IN THE CNS AND PNS OF FA MODEL MICE

After AAV-genome sequence verification, we conducted large-scale virus preps of AAV- B10S packaging FXNm or mNeonGreen under the FXN promoter for testing in vivo. After assessing their baseline behavioral performance as described in the next section, we injected a cohort of 4-5 symptomatic adult FXNiKD or WT mice per group with a combination of AAV.SB10:FXNm or control, each virus at a concentration of 1×10^{11} vg/mouse. The mice were behaviorally tested every two weeks until they reached the experimental endpoint at 6 weeks post injection, at which point the mice were euthanized and perfused for IHC analysis of FXN expression. FXN expression was confirmed by IHC staining for FLAG in the brain and DRGs (Figure 6), as well as cardiac tissue and liver (data not shown). Due to the expression patterns observed in earlier experiments in this study, we expected that combining more targeted delivery with a FXN construct containing regulatory elements of the native gene would lead to physiologically relevant patterns of transduction in the nervous system, with the added benefit of minimizing off target transduction. In the cerebellum, we were encouraged by the transduction pattern which included strong expression in neurons in the deep cerebellar nuclei and the granular layer. Transduction of the PNS by AAV-PHP.S delivery of FXNm, as shown in the right panel of Figure 4, is consistent with what we had observed in the KIKO mice tested with AAV-PHP.SN.

To evaluate the effectiveness of these viruses in preventing or alleviating the symptoms and pathologic features of FA, we administered AAV-FXNm and measured motor performance in an inducible shRNA knockdown model of FA, which exhibits severe symptoms affecting organ systems resembling human patient disease progression (Chandran 2017).

COMBINED GENE REPLACEMENT IS REQUIRED IN BOTH THE CENTRAL AND PERIPHERAL NERVOUS SYSTEMS TO PREVENT MOTOR PROGRESSION IN AN INDUCIBLE MODEL OF FRIEDREICH'S ATAXIA

We tested the therapeutic efficacy of AAV-CAP-B10S:FXNm vectors in the FXNiKD mouse model of FA, which is reported to exhibit robust behavioral and physiologic phenotypes (Chandran 2017). Motor phenotypes emerged after 8-12 weeks on the mild doxycycline regimen, including coordination deficits as measured by the narrowing beam test and overall mortality. In the narrowing beam test, mice are placed on the wide end of a progressively narrowing beam, and walk along the beam to return to their home cage. We observed that mice with coordination deficits take more time to traverse the beam, and may misplace their paws so that they slip off of the beam surface. Both the time to cross and the number of foot faults are recorded.

After measuring behavioral baseline performance on gait, balance and coordination tasks and observing the onset of an ataxic phenotype in adult FXNiKD mice, we injected an age and sex matched symptomatic pilot cohort (n=4-5 per group) with AAV- B10S packaging AAV genomes encoding either FXNm or mNeonGreen under the putative FXN promoter as a control. We monitored the mice for 6 weeks, measuring performance on motor tasks and monitoring cardiac function using ECG at the end of the testing period. These mice were then euthanized, perfused, and tissue was harvested for analysis. In this late intervention cohort, neither the administration of the therapeutic or control virus had any effect on the survival or motor and physiologic phenotypes we had observed as a result of knocking down endogenous frataxin expression. Within two weeks of administration, the knockdown mice began to exhibit worsening coordination, poor health, and death. This reaction was restricted to knockdown mice, and WT controls were unaffected. Thus we deemed a dosage-toxicity problem to be unlikely. Interestingly, the knockdown mice that were the most affected were males. As a result, we were unable to collect much data on post-treatment male mouse performance, and our conclusions are drawn from data we collected from surviving female knockdown mice.

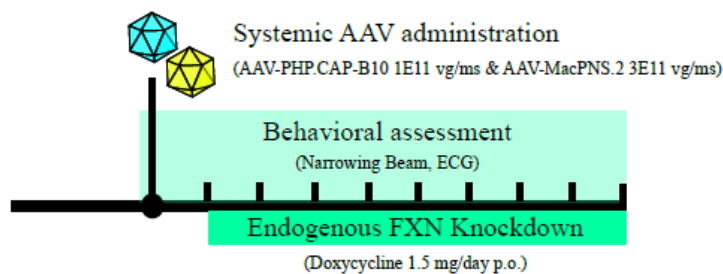
As it was unclear whether this model, and particularly the male mice, have a unique susceptibility to toxicity stemming directly from the intervention, or whether this severe phenotype is a manifestation of the disease course in this model, we first hypothesized that as this is a degenerative condition, the timing of our intervention was too late to rescue the motor phenotypes and cell health caused by knocking down endogenous expression of FXN. To test this line of reasoning, we are expanding our colony to conduct the same experiment in 4-6 week old mice, but this time, to perform the AAV administration prior to initiating shRNA knockdown.

PROPHYLACTIC AAV-FXN DELIVERED TO THE PNS AND CNS SIMULTANEOUSLY PREVENT ONSET OF THE MOTOR DEGENERATIVE PHENOTYPE UPON INDUCTION OF NATIVE FXN KNOCKDOWN

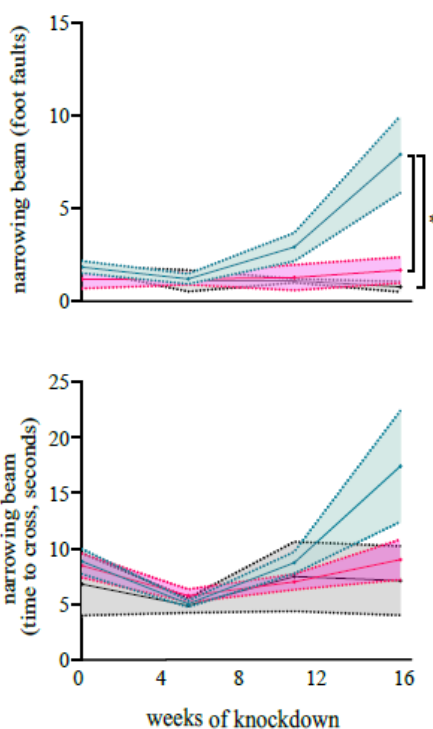
FXNiKD mice were genotyped and divided into age and sex matched groups for treatment with AAV-FXN or AAV-mNeonGreen to control for the potential effects of the capsid injection or nonspecific transgene effects. Wildtype littermates were included as a healthy control group. These mice were systemically treated with a cocktail of CAP.B10 and PNS2 at a total titer of 4×10^{11} viral genomes per mouse at 6-8 weeks of age, and baseline behavior measurements were recorded, and the researcher was blinded. After a two week expression period, doxycycline diet was initiated, in which the rodent chow was replaced with doxycycline containing food, and the water was replaced with doxycycline containing water with sucrose (2 mg/mL doxycycline in 5% sucrose). The doxycycline dosage for effective knockdown with gradual phenotypic onset was determined empirically on a pilot cohort from the same colony. Mice were then behaviorally and physiologically monitored as described above, prior to tissue analysis.

Over the course of the experiment, motor coordination as measured by the narrowing beam task deteriorated in the group injected with AAV-mNeonGreen, while the group injected with AAV-FXN performed near wildtype to the experimental endpoint.

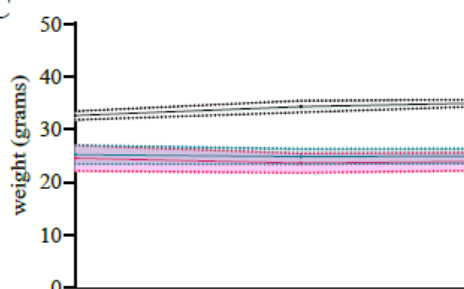
A



B



C



D

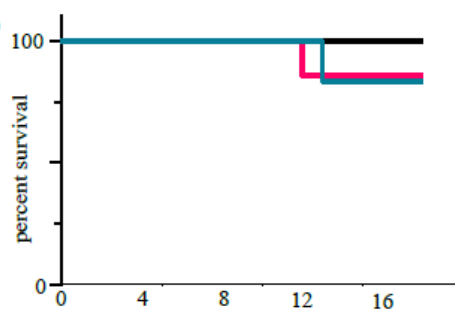


Figure 2.6. Prophylactic AAV-FXN prevents progression of sensorimotor deterioration in the narrowing beam task. (A) Experimental schematic. CNS targeting via AAV-PHP.CAP.B10 and PNS targeting via AAV-MacPNS.2 were combined to deliver either FXNm cargo (magenta) or an mNeonGreen control cargo (teal). (B) Narrowing Beam assay (students t-test, $p=0.05$), (C) longitudinal weight and (D) survival are reported ($n=6-7$ per group, young adult mice from FXNiKD line and untreated wildtype littermates (black)).

PROPHYLACTIC AAV-FXN PREVENTS QT INTERVAL PROLONGATION AND FIBROSIS OF CARDIAC MUSCLE IN FXN^{KD} KNOCKDOWN MICE

In addition to the motor phenotype, mouse cardiac physiology was assessed in the same time course cohort. After receiving prophylactic AAV-FXN or control, animals underwent periodic electrocardiogram measurement under anesthesia across lead II. At the study endpoint, traces were analyzed to assess measures associated with human FA pathophysiology, including any measures that support a hypertrophic cardiomyopathy picture. When compared with wildtype animals, several animals which received the control treatment exhibited traces with elongated or double-peaked Q waves, prolonged QT intervals, and increased fibrosis of the cardiac muscle as measured by Masson Trichrome staining. By contrast, those mice treated with AAV-FXN had normal appearing traces and no prolongation of the QT interval compared to wildtype healthy animals (Figure 2.7). This exciting finding adds support to the use of systemic gene replacement for FA, and the potential for mediating multisystem improvement of morbidity and mortality associated phenotypes with a single treatment.

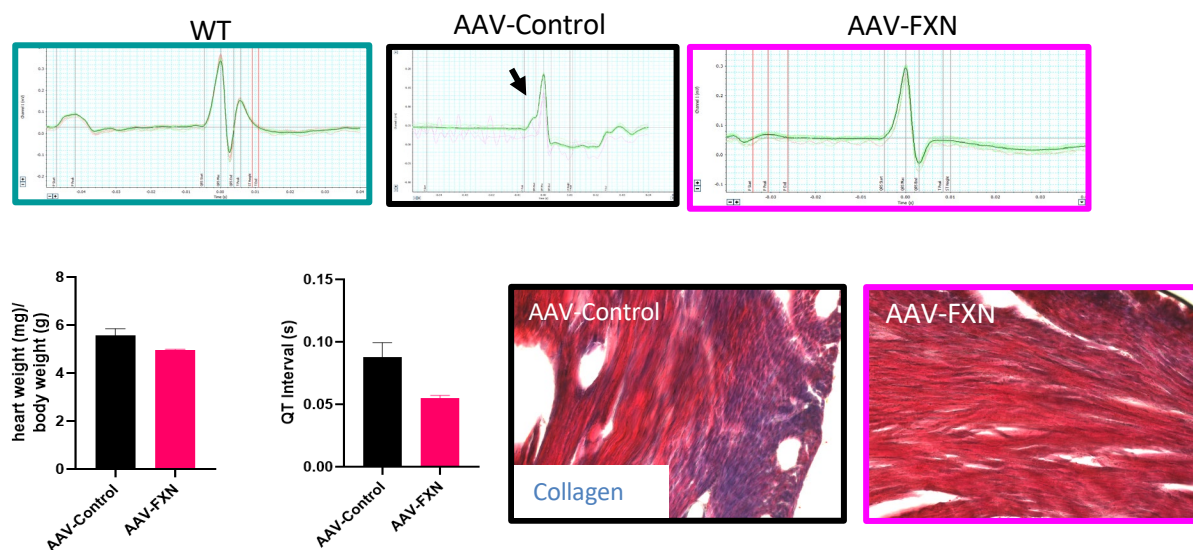


Figure 2.7. Electrocardiogram shows trend toward prolongation of the QT interval in control animals, with greater collagen deposition in cardiac muscle at endpoint. A) Representative traces from ECGs within each group. Black arrow denotes double peak inflection in QRS complex. B) QT intervals and gross tissue weight in AAV control and AAV FXN animals. C) Fibrosis as measured by collagen deposition in murine cardiac tissue. N=6-7 per group.

In addition to postmortem cardiac staining, we stained the mouse brains from the behavior cohort to validate AAV-FXN expression durability and penetrance in target tissues. We observed mostly neuronal transduction (greater than 50% of the brain cells transduced were neurons), and of the neurons, roughly 55% were strongly transduced. Within the dentate nucleus and Dorsal Root Ganglia, these estimates hovered around 40% of DAPI positive cells (Figure 2.8). Liver analysis showed very little transduction (data not shown).

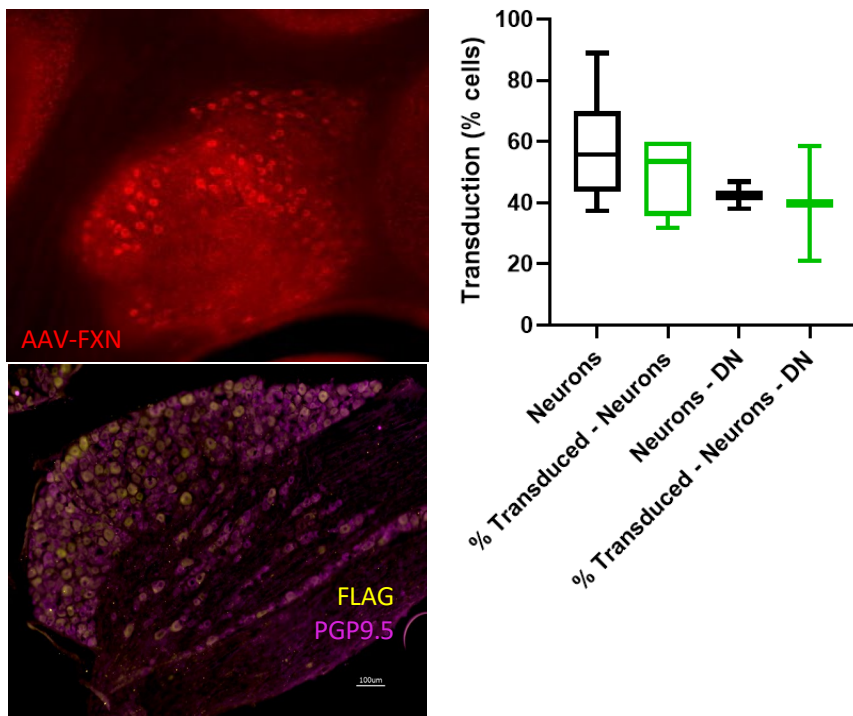


Figure 2.8. Transduction rates in cerebellar and peripheral nervous system target tissues. Behavior cohort results were achieved with expression in 40% of neurons transduced in the dentate nucleus (DN). Staining of DN is for FXN, Staining in DRG is for FLAG.

Encouraged by these findings, we then asked if more resolution on the mechanism of rescue could be obtained by separating the treatment into central and peripheral components. In addition to providing insight into the rescue mechanism, this experiment would also disentangle a major pathophysiology question of the pattern of degeneration observed in FA: do the CNS and PNS degeneration happen intrinsically and independently, is PNS degeneration causing loss of sensory input, leading to atrophy in the CNS, or is CNS degeneration causing loss of input to the PNS, resulting in atrophy there? We sought to answer this question by decoupling the delivery to the CNS and PNS target tissues, using separate injections of either AAV.CAP-B10 or AAV-PNS2, and repeating the measures as outlined in the previous experiment.

We found that prophylactic treatment decoupling administration of peripheral and central targeting capsids (one capsid or the other) fails to prevent the onset of the motor phenotype completely (Figure 2.9 B). Thus, both central and peripheral targeting is required for rescuing the motor coordination phenotype in the FXNiKD line. This observation is not surprising, as both the cerebellar and sensory centers are required for the coordination of movements requiring proprioceptive input, and is suggestive of a globally stressful condition within nervous system tissues when functional Fxn is depleted.

We also investigated the effect on the cardiac phenotype observed in the combination treatment group, to see which capsid may have been responsible for the rescue of this phenotype. We had hypothesized that it was possible that rescue was a direct result of muscle transduction, as both vectors are from parent vectors that are known to transduce heart muscle (REF). However, we were interested in the possibility that because cardiac rhythm events are common in human FA patients, there may be a nervous input, whether sympathetic or otherwise, that may play a role in pathology. Upon evaluation of ECG data from each group, we observed a transient increase of the QT interval

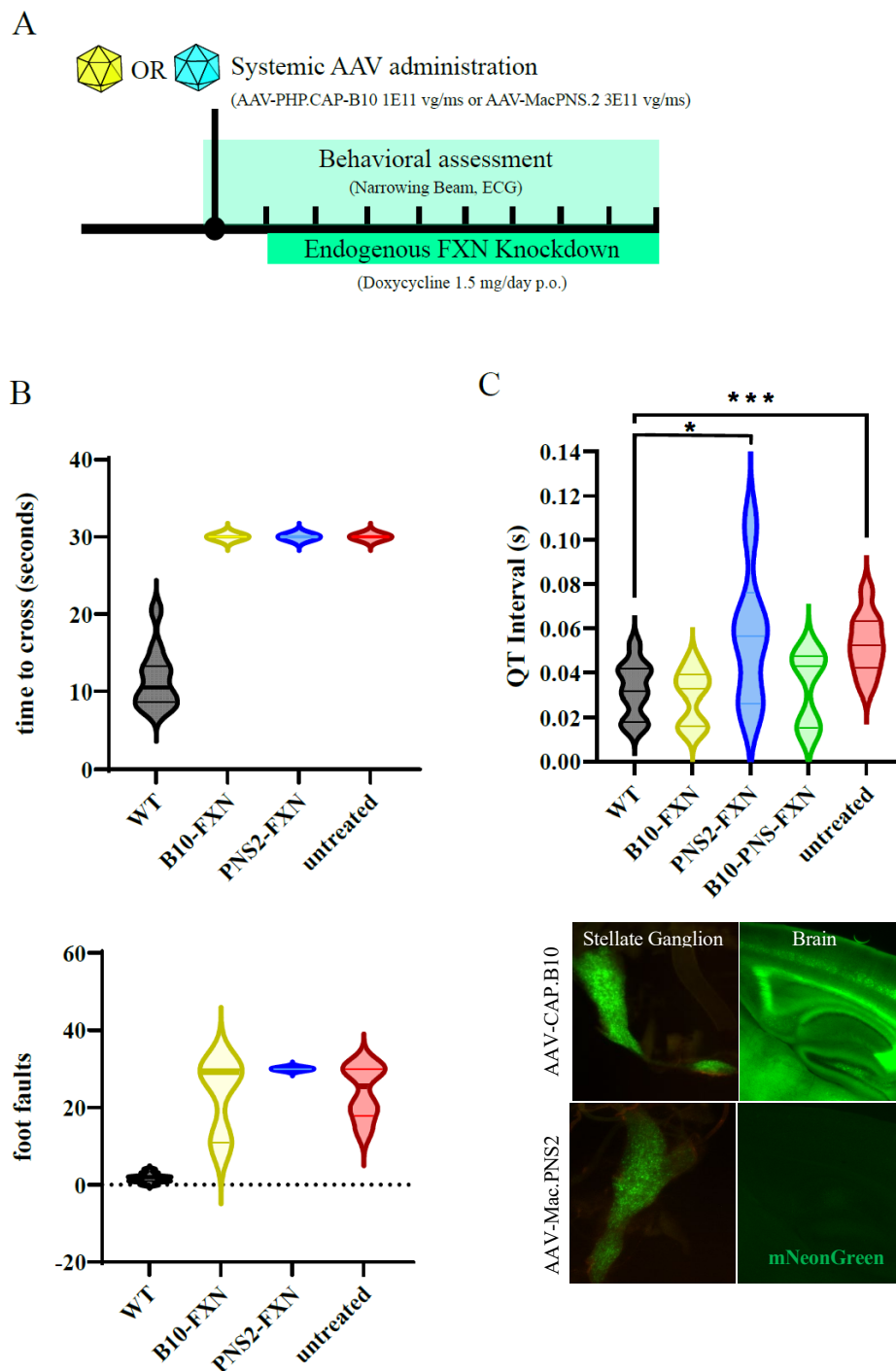


Figure 2.9. Individually injected vectors delivering FXN to the CNS or PNS fail to outperform untreated animals in sensorimotor tasks, but CNS delivery is required to rescue cardiac manifestations of FXN loss. (A) Experimental design. Groups: wildtype (n=18), AAV-CAP.B10 only (n=8), AAV-MacPNS.2 (n=8), dual vector treatment (n=6), and untreated FXNiKD (n=9). (B) Narrowing beam task shows no difference between singly treated groups and untreated disease animals. (C) CNS-delivered AAV-FXN rescues cardiac physiology deficit of untreated animals as measured by QT interval, statistics by t-test (D) Characterization of nervous input to the heart by each CNS and PNS capsid. RO administration, 5E11 vg/mouse, 3 weeks expression. N=4 mice per capsid

eliminating the prolonged QT phenotype observed in the untreated animals and control animals in the prior experiment (Figure 2.9C). This suggested a centrally mediated effect on cardiac physiology, rather than an intrinsic effect in the cardiac muscle. This led us to investigate the role of central and peripheral structures related to cardiac function, and whether mechanistically, delivery could explain the differences, and found that both capsids surprisingly transduce the stellate ganglion, which governs sympathetic input to the heart, while CAP.B10 is the only capsid of the two that transduces central structures (Figure 2.9D). Given that transduction of the heart muscle itself is similar with the two capsids, we reasoned that the cardiac phenotypic benefit may be driven by central mechanisms rather than peripherally mediated.

DISCUSSION

In this study, we developed and evaluated a precision gene therapy approach to prevent and treat the pathologic features in a mouse model of FA. Our approach achieves its precision by utilizing highly specialized delivery vehicles to deliver gene therapy cargo that contains the nuanced control mechanisms of a normal, functional human frataxin gene found in healthy individuals. We observed that the top therapeutic gene construct we created expresses frataxin in the same brain regions where it is highly expressed in normal mice, and where it has been observed to be deficient in patients with Friedreich's Ataxia. In addition, we observed that our delivery vehicles deliver this construct to the dorsal root ganglion cells, where we observed expression, another key therapeutic target in FA. To evaluate efficacy, we ran two experiments: one with combined delivery to the CNS and PNS, and one with independent delivery to each, and found that it is necessary to treat both the CNS and PNS to prevent the motor phenotype onset, but that it is possible that rescue of the cardiac phenotype may be mediated through the CNS. Additionally, we observed a transient cardiac response that begins by worsening, but then resolves completely to healthy wildtype levels. The timing and nature of this observation is consistent with cardiac remodeling after a viral insult, but more work would be needed to follow up on whether this is an inflammatory process or is driven by some other compensatory mechanism.

CHAPTER 2 REFERENCES

Campuzano, V., Montermini, L., Moltò, M.D., Pianese, L., Cossée, M., Cavalcanti, F., Monros, E., Rodius, F., Duclos, F., Monticelli, A., et al. (1996). Friedreich's ataxia: autosomal recessive disease caused by an intronic GAA triplet repeat expansion. *Science* 271, 1423–1427.

González-Cabo, P., and Palau, F. (2013). Mitochondrial pathophysiology in Friedreich's ataxia. *J. Neurochem.* 126 *Suppl* 1, 53–64.

Koeppen, A.H. (2011). Friedreich's ataxia: pathology, pathogenesis, and molecular genetics. *J. Neurol. Sci.* 303, 1–12.

Piguet, F., de Montigny, C., Vaucamps, N., Reutenauer, L., Eisenmann, A., and Puccio, H. (2018). Rapid and Complete Reversal of Sensory Ataxia by Gene Therapy in a Novel Model of Friedreich Ataxia. *Mol. Ther.* 26, 1940–1952.

Perdomini, M., Belbellaa, B., Monassier, L., Reutenauer, L., Messaddeq, N., Cartier, N., Crystal, R.G., Aubourg, P., and Puccio, H. (2014). Prevention and reversal of severe mitochondrial cardiomyopathy by gene therapy in a mouse model of Friedreich's ataxia. *Nat. Med.* 20, 542–547.

Huichalaf, C., Perfitt, T.L., Kuperman, A., Gooch, R., Kovi, R.C., Brenneman, K.A., Chen, X., Hirehallur-Shanthappa, D., Ma, T., Assaf, B.T., et al. (2022). In vivo overexpression of frataxin causes toxicity mediated by iron-sulfur cluster deficiency. *Mol Ther Methods Clin Dev* 24, 367–378.

Belbellaa, B., Reutenauer, L., Messaddeq, N., Monassier, L., and Puccio, H. (2020). High Levels of Frataxin Overexpression Lead to Mitochondrial and Cardiac Toxicity in Mouse Models. *Mol Ther Methods Clin Dev* 19, 120–138.

Zlokovic, B.V., and Apuzzo, M.L. (1997). Cellular and molecular neurosurgery: pathways from concept to reality--part II: vector systems and delivery methodologies for gene therapy of the central nervous system. *Neurosurgery* *40*, 805–812; discussion 812–813.

Chan, K.Y., Jang, M.J., Yoo, B.B., Greenbaum, A., Ravi, N., Wu, W.-L., Sánchez-Guardado, L., Lois, C., Mazmanian, S.K., Deverman, B.E., et al. (2017). Engineered AAVs for efficient noninvasive gene delivery to the central and peripheral nervous systems. *Nat. Neurosci.* *20*, 1172–1179.

Ravindra Kumar, S., Miles, T.F., Chen, X., Brown, D., Dobрева, T., Huang, Q., Ding, X., Luo, Y., Einarsson, P.H., Greenbaum, A., et al. (2020). Multiplexed Cre-dependent selection yields systemic AAVs for targeting distinct brain cell types. *Nat. Methods* *17*, 541–550.

Challis, R.C., Ravindra Kumar, S., Chen, X., Goertsen, D., Coughlin, G.M., Hori, A.M., Chuapoco, M.R., Otis, T.S., Miles, T.F., and Gradinaru, V. (2022). Adeno-Associated Virus Toolkit to Target Diverse Brain Cells. *Annu. Rev. Neurosci.* *45*, 447–469.

Goertsen, D., Flytzanis, N.C., Goeden, N., Chuapoco, M.R., Cummins, A., Chen, Y., Fan, Y., Zhang, Q., Sharma, J., Duan, Y., et al. (2022). AAV capsid variants with brain-wide transgene expression and decreased liver targeting after intravenous delivery in mouse and marmoset. *Nat. Neurosci.* *25*, 106–115.

Deverman, B.E., Pravdo, P.L., Simpson, B.P., Kumar, S.R., Chan, K.Y., Banerjee, A., Wu, W.-L., Yang, B., Huber, N., Pasca, S.P., et al. (2016). Cre-dependent selection yields AAV variants for widespread gene transfer to the adult brain. *Nat. Biotechnol.* *34*, 204–209.

McMackin, M.Z., Henderson, C.K., and Cortopassi, G.A. (2017). Neurobehavioral deficits in the KIKO mouse model of Friedreich's ataxia. *Behav. Brain Res.* *316*, 183–188.

Chandran, V., Gao, K., Swarup, V., Versano, R., Dong, H., Jordan, M.C., and Geschwind, D.H. (2017). Inducible and reversible phenotypes in a novel mouse model of Friedreich's Ataxia. *Elife* *6*. 10.7554/eLife.30054.

Chuapoco, M.R., Flytzanis, N.C., Goeden, N., Christopher Octeau, J., Roxas, K.M., Chan, K.Y., Scherrer, J., Winchester, J., Blackburn, R.J., Campos, L.J., et al. (2023). Adeno-associated viral vectors for functional intravenous gene transfer throughout the non-human primate brain. *Nat. Nanotechnol.* *18*, 1241–1251.

*Chapter 3*DELIVERY AGNOSTIC EXPRESSION REGULATION TO CIRCUMVENT
OVEREXPRESSION TOXICITY

This chapter contains work from this referenced manuscript:

Michael J. Flynn, Acacia M.H. Mayfield, Rongrong Du, Viviana Gradinaru, Michael B. Elowitz. Synthetic dosage-compensating miRNA circuits allow precision gene therapy for Rett syndrome. bioRxiv 2024.03.13.584179; doi: <https://doi.org/10.1101/2024.03.13.584179>

ABSTRACT

A longstanding challenge in gene therapy is expressing a dosage-sensitive gene within a tight therapeutic window. For example, loss of *MECP2* function causes Rett syndrome, while its duplication causes *MECP2* duplication syndrome. Viral gene delivery methods generate variable numbers of gene copies in individual cells, creating a need for gene dosage-invariant expression systems. Here, we introduce a compact miRNA-based, incoherent feed-forward loop circuit that achieves precise control of *Mecp2* expression in cells and brains, and improves outcomes in an AAV-based mouse model of Rett syndrome gene therapy. Single molecule analysis of endogenous and ectopic *Mecp2* mRNA revealed precise, sustained expression across a broad range of gene dosages. Delivered systemically in a brain-targeting AAV capsid, the circuit strongly suppressed Rett behavioral symptoms for over 24 weeks, outperforming an unregulated gene therapy. These results demonstrate that synthetic miRNA-based regulatory circuits can enable precise in vivo expression to improve the safety and efficacy of gene therapy.

INTRODUCTION

Gene therapy promises to enable lasting cures for genetic diseases by delivering corrected copies of genes mutated within a patient. Recently, the field has achieved clinical successes addressing spinal muscular atrophy (SMA) (Mendell et al. 2017), hemophilia (Nathwani et al. 2014, George et al. 2017, Ozelo et al. 2022) and inherited retinal dystrophy (Russell et al. 2017), with other applications in the pipeline (Mendell et al. 2021). New technologies, such as adeno-associated viral vectors (AAVs) that target specific cell types at high efficiency (Challis et al. 2022), may accelerate progress in the coming decade.

However, many gene therapies face a ‘Goldilocks’ problem: too little expression of the gene leads to the disease phenotype, but too much expression can induce other disease phenotypes. For example, loss of function of the *SYNGAP1* gene results in non-syndromic intellectual disability and epilepsy (Berryer et al. 2013) while overexpression of *SYNGAP1* leads to a pronounced depression of excitatory signaling in vitro (Rumbaugh et al. 2006). Similarly, *UBE3A* deficiency causes Angelman’s syndrome, but duplication and triplications are associated with autism spectrum disorder (Smith et al. 2011). Overexpression toxicity is also a concern in clinical gene replacement. For example, loss of function mutations in *SMNI* cause spinal muscular atrophy, but overexpression of *SMNI* through gene therapy led to clinically silent but concerning dorsal root ganglion pathology in mouse and non-human primate studies of SMA gene therapy (Van Alstyne et al. 2021; Hinderer et al. 2018; Hordeaux et al. 2020).

Rett syndrome presents the prototypical Goldilocks problem. It is a severe neurodevelopmental disease caused by loss-of-function mutations in the gene encoding MeCP2, a methyl-CpG/A binding protein (Amir et al. 1999). MeCP2 binds to methylated regions of the genome and serves as a binding hub and bridge to the NCoR/SMRT co-repressor complex to repress methylated genes, an essential function for brain maturation (Tillotson and Bird 2019). Since *MECP2* is on the X chromosome, mutations in the gene lead to different symptoms between males and females.

Human males cannot survive with a single non-functional copy of *MECP2* (Villard et al. 2000). In human females heterozygous for a mutation in *MECP2*, Rett syndrome is characterized by a severe developmental regression at 7-18 months of age, progressive loss of speech and hand use, ataxia, and acquired microcephaly, among other symptoms (Hagberg et al. 1983). MeCP2-deficient male mice show reductions in lifespan, brain size, neuron soma size, synapse counts, dendritic spine density, and electrophysiological activity (Tropea et al. 2009). However, mild overexpression of MeCP2 also leads to a disease phenotype (Collins et al. 2004) and duplication of the *MECP2* gene causes another disorder, *MECP2* duplication syndrome (Ramocki et al. 2009). In engineered mice, Cre-based reactivation of *Mecp2* expression from its endogenous genomic context alleviates disease phenotypes, suggesting that the condition is reversible (Guy et al. 2007). However, gene therapies based on AAV-mediated delivery of *Mecp2* to Rett model mice have induced toxicity (Gadalla et al. 2013, Gadalla et al. 2017, Sinnott et al. 2017, Matagne et al. 2017, Tillotson et al. 2017, Matagne et al. 2021) specifically from overexpression of the MeCP2 protein (Gadalla et al. 2017). Thus, a critical requirement for Rett syndrome gene therapy is to express MeCP2 within a narrow therapeutic window.

In this work, we designed a synthetic biological circuit that provides this capability, and demonstrated that it can improve Rett syndrome gene therapy in vivo. This compact miRNA-based incoherent feedforward loop (IFFL) circuit limited *Mecp2* expression and reduced its sensitivity to gene dosage in cell culture. Further, it restricted ectopic *Mecp2* mRNA to levels comparable to, but not exceeding, those of endogenous *Mecp2* in the mouse brain. Finally, a gene therapy vector containing the circuit outperformed unregulated gene therapy, improving behavioral symptoms over a timescale of 24 weeks. These results demonstrate that an integrated miRNA-based gene circuit can improve gene therapies for Rett syndrome and likely for other genetic diseases as well.

RESULTS

MODELING PREDICTS INCOHERENT FEEDFORWARD REGULATION CAN TUNE PROTEIN EXPRESSION TO WITHIN A THERAPEUTIC WINDOW

Expression patterns of ectopic genes may deviate significantly from the endogenous distribution of expression for several reasons. First, the number of gene copies delivered to an individual cell can vary by orders of magnitude due to varying uptake efficiency of different organs and cell types (**Figure 1A**, upper right) (Nathwani et al. 2011, Wang et al. 2020), spatial gradients around a direct injection site (**Figure 1A**, bottom left) and Poisson-distributed stochastic vector uptake by individual cells (**Figure 1A**, bottom right) (Prasad et al. 2011). Second, engineered promoters typically used in gene therapy vectors often induce stronger expression than endogenous promoters, potentially leading to toxicity from even a single copy (**Figure 1B**, left panel) (Huichalaf et al. 2022). Finally, for an X-linked disease such as Rett syndrome, cells may express either zero or one copy of the endogenous gene due to X inactivation. Thus, even if an ectopic gene is expressed at the physiological levels this could still lead to overexpression in cells that express the endogenous copy (**Figure 1B**, right panel).

Current approaches to limiting ectopic expression include optimizing the promoter or incorporation of target sites for endogenous miRNAs (Sinnott et al. 2021). However, while these approaches generally reduce mean expression relative to unregulated constructs, they cannot actively adapt to variation in gene dosage.

The incoherent feedforward loop (IFFL) is an adaptive biological circuit motif that could address these challenges (Frei et al. 2021, Mangan et al. 2003). Previous work has shown that synthetic IFFL circuits can successfully buffer gene expression against variations in gene dosage (Bleris et al. 2011, Segall-Shapiro et al. 2018, Lillacci et al. 2018, Jones et al. 2020), noise from upstream regulators (Osella et al. 2011), competition for cellular resources (Jones et al. 2020, Frei et al. 2020), or general perturbations (Strovas et al. 2014). Here, we consider IFFLs in which a target gene and its negative regulator are co-transcribed, so that higher gene dosage leads to greater transcription rates of both components (**Figure 1C**) (Frei et al. 2021, Mangan et al. 2003, Khammash et al. 2021). A simple mathematical model of such an IFFL showed that, above a minimal expression level, the two effects can cancel out to maintain a fixed mean expression level

of the target gene across a wide range of gene dosages (**Figure 1D, Methods**). We further extended this model to incorporate discrete gene copy numbers, stochastic vector delivery, and bursty gene expression kinetics. We also incorporated a strong promoter so there is overexpression at even a single copy. Simulated IFFLs operating in these regimes successfully regulated the distribution of expression to be similar to a target endogenous distribution, across different MOIs (**Figure 1E, Methods**). These results suggested that a suitably engineered IFFL could generate a more robust gene therapy expression system.

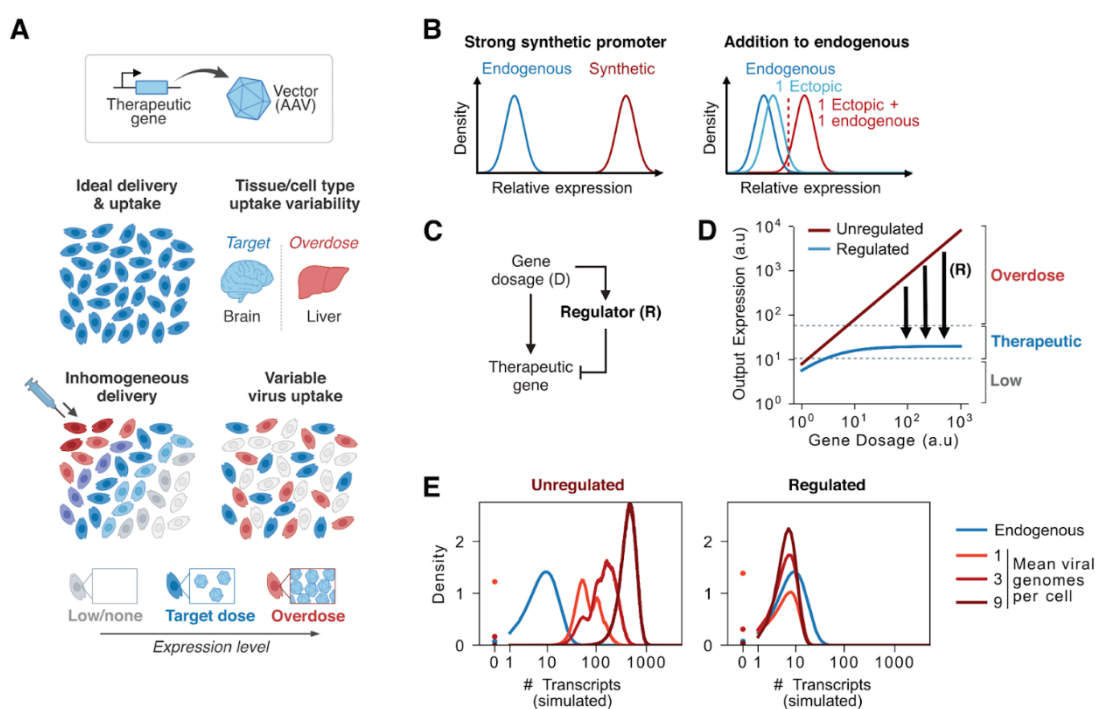


Figure 1. Mathematical modeling predicts that incoherent feedforward loop circuits can maintain gene expression within a therapeutic window.

(A) Gene therapy contends with multiple sources of variability in expression. Ideally, all cells would receive the same number of viral genome copies, and express the correct amount of the therapeutic gene (upper left). However, viral uptake rates can vary greatly by organ and cell type (upper right), such that a dose that is therapeutic in one organ (e.g. brain, blue) may be toxic in another that takes up viral vectors

at a higher rate (e.g. liver, red). With direct injection, cells close to the injection site receive more copies than cells farther away (lower left). Finally, even with correct mean delivery, viral uptake remains subject to stochastic variation (lower right).

(B) The high level of expression induced by synthetic promoters commonly used in gene therapy may cause toxic overexpression from even a single transgene copy (left). Additionally, for X-linked genes like *MECP2*, approximately half of cells in affected females express a fully functioning endogenous copy. The gene therapy must not overexpress MeCP2 when its expression is added to the wildtype allele (right).

(C) Schematic of an incoherent feedforward loop motif in which a therapeutic gene is co-expressed with its own negative regulator.

(D) Therapeutic gene expression as a function of gene dosage, as modeled for an idealized IFFL. The increasingly negative action of the repressor (R, black) compensates for increases in gene dosage, leading to regimes where large changes in gene dosage yield nearly the same output expression of the circuit (blue), preventing overexpression.

(E) Simulated distributions of therapeutic gene expression at different viral MOI, either unregulated (left) or regulated by an IFFL (right), compared to a target endogenous expression distribution (blue). Simulations incorporate stochastic viral uptake, bursty transcription, and stochastic enzyme kinetics as well as an offset between single-copy expression and the endogenous level of a therapeutic gene. The IFFL circuit compensates for these sources of variation.

A SYNTHETIC HOST-TARGETING MIRNA MODULE ENABLES DOSAGE COMPENSATION OF *MECP2* EXPRESSION

In some natural genes, intronic miRNAs downregulate expression of their host gene, forming an IFFL within a single transcript (Chamorro-Jorganes et al. 2014, Tsange et al. 2007, Mrgraw et al. 2010). This circuit architecture has also been demonstrated synthetically (Bleris et al. 2011) and could have desirable properties for gene therapy, since intronic miRNA expression cassettes are non-immunogenic and genetically compact. However, it has not been established if synthetic

miRNA-based IFFLs can match the expression level of an endogenous mRNA, or whether they can improve the function of an AAV-based gene therapy.

To address these questions, we designed a set of miRNA-based dosage compensating IFFL constructs (**Figure 2A**). We engineered a divergent promoter made up of the CMV enhancer flanked by the MeP229 promoter (Gadalla et al. 2013) in the forward direction and an intron-free Efl α promoter in the reverse direction ('ECM promoter'). The forward promoter drives expression of a previously characterized MeCP2-EGFP protein fusion to facilitate analysis of protein expression (Tillotson et al. 2017). The reverse promoter drives expression of unregulated mRuby3 as an indicator of gene dosage.

To implement IFFL regulation, we incorporated a miRNA expression cassette in a synthetic intron (Qiu et al. 2008) within the 3'UTR of *Mecp2-EGFP*. This miRNA cassette is based on the strong and well-characterized miR-E backbone (Fellmann et al. 2013), which generates a miRNA complementary to a 21-bp sequence derived from *Renilla luciferase*, which is orthogonal to the human genome. To compare two different strengths of regulation, we inserted either 1 or 4 copies of the target sequence into the 3'UTR, upstream of the miRNA-containing intron, to create "1x" and "4x" circuits (**Figure 2A**). We also constructed an "unregulated" control construct lacking both the miRNA and its target sites. All 3 constructs were less than 4300 base pairs in length, and thus small enough to be efficiently packaged inside an AAV.

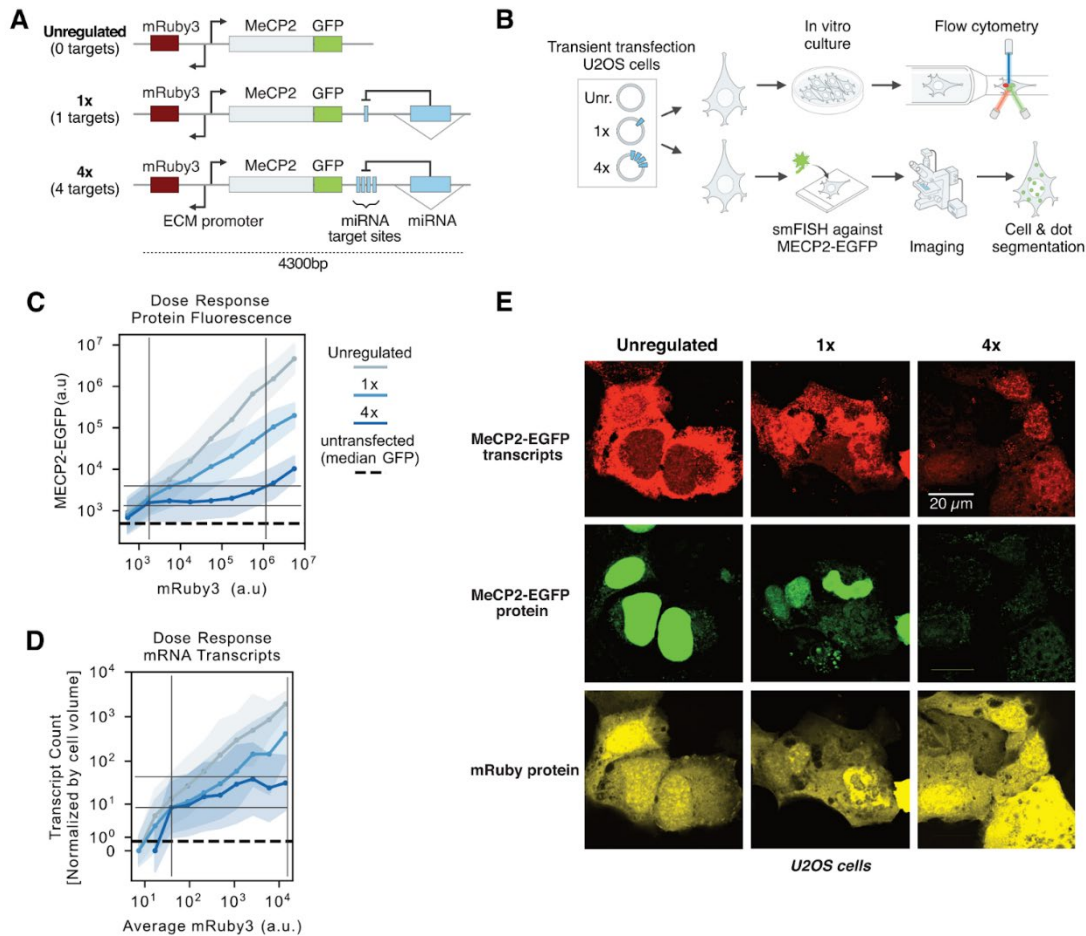


Figure 2. Synthetic miRNA IFFLs can adapt to variations in gene dosage in cell culture.

(A) Designs of 3 constructs based on a divergent promoter producing MeCP2-EGFP in the forward direction and the mRuby3 dosage indicator in the reverse. The first circuit, labeled “unregulated”, has no miRNA targets and no miRNA cassette and serves as an unregulated control. The second (1x) and third (4x) circuits contain a miRNA cassette located within a synthetic intron in the 3’ UTR of *Mecp2-EGFP*, which respectively targets 1 or 4 fully complementary miRNA target sites upstream of the intron. All constructs are less than 4300 bp and fit inside an AAV.

(B) Workflow to characterize circuit performance at both the mRNA and protein levels. For protein, U2OS cells were transiently transfected, cultured for 48 hours, and had protein expression measured by

flow cytometry (upper path). For mRNA, U2OS cells were transiently transfected, incubated for 48 hours, fixed, and then analyzed with smFISH and confocal microscopy (lower path).

(C) MeCP2-EGFP protein fluorescence as a function of mRuby3 dosage indicator for the 3 constructs, as measured by flow cytometry. MeCP2-EGFP was proportional to dosage for the unregulated construct (gray), as expected. For the 1x construct (medium blue), the slope was reduced, indicating a decreased responsiveness to dosage. For the 4x construct (dark blue), MeCP2-EGFP expression was nearly independent of dosage over 2.5 orders of magnitude variation in gene dosage (framed region). This stable expression level was approximately 3-fold above the fluorescence of untransfected cells (dashed black line). Here, and in D, shaded regions represent ± 1 standard deviation of the logarithmic expression values.

(D) *Mecp2-EGFP* transcript count as a function of average mRuby3 fluorescence, as measured by smFISH and confocal microscopy. The relationship between *Mecp2-EGFP* transcripts and dosage indicator fluorescence largely agreed with the protein-level results for each construct. The 4x construct produced an expression level that varied less than 4-fold over a greater than 300-fold range of dosage (framed region).

(E) smFISH imaging of ectopic *Mecp2-EGFP* transcripts (upper row) and protein (middle row), as well as mRuby dosage indicator (lower row). Cells displayed comparable levels of mRuby protein in all conditions (bottom row), while *Mecp2-EGFP* expression decreases with stronger IFFL regulation at both transcript (upper) and protein (middle) levels.

To test the ability of these circuits to compensate for variation in gene dosage, we quantified their expression as a function of dosage at the protein and mRNA levels. For protein-level quantification, we transiently transfected U2OS cells and analyzed MeCP2 expression using flow cytometry (**Figure 2B**, upper path, **Methods**). Unregulated MeCP2 was expressed at a level proportional to gene dosage, as expected (**Figure 2C**). The 1x construct reduced MeCP2-EGFP expression and its dependence on dosage (slope of EGFP versus mRuby3) (**Figure 2C**). While it did not achieve complete dosage compensation, it provided a useful intermediate-regulation condition for subsequent studies. The 4x circuit generated behavior closer to that expected from

the simplified IFFL model (**Figure 1D**), with relatively constant (<3-fold variation) expression across a broad range (>300-fold) of gene dosage (**Figure 2C**).

To quantify these differences in expression at the mRNA level, we transiently transfected U2OS cells with each construct, performed smFISH (Takei et al. 2021) against the *Mecp2-EGFP* transcript, and imaged both protein fluorescence and transcripts using confocal microscopy (**Figure 2B**, lower path, **Methods**). Consistent with the flow cytometry results, among cells expressing similar levels of the mRuby dosage reporter, MeCP2-EGFP mRNA and protein expression levels decreased with increasing number of miRNA target sites (**Figure 2E**).

To quantitatively measure the relationship between gene dosage and target mRNA levels, we computationally segmented cells in the smFISH images and counted individual transcripts (dots in **Figure 2E**, **Methods**). The unregulated and 1x constructs showed linear and sublinear, but still increasing, dependence on the mRuby3 dosage indicator, respectively (**Figure 2D**). The 4x construct exhibited the lowest level of expression, which also varied less than 4-fold over a greater than 300-fold range of dosage (**Figure 2D**).

To test for potential off-target effects of the miRNA regulation, we performed bulk-RNAseq and compared transcriptome expression of a BFP-miRNA (miR-E) cassette to a negative control transfection of a BFP-only expression vector (**Methods**). Few genes were relatively up- or down-regulated in the miRNA condition and none contained partial sequence matches to the miRNA (**Supplementary Figure 1**). These results suggest any sequence-specific perturbations from the synthetic miRNA itself were minimal.

Taken together, these results indicate that the 4x IFFL circuit can establish dosage-insensitive expression and reduce the magnitude of cell-cell variation in gene expression in vitro, without perturbing endogenous gene expression.

AAV-DELIVERED IFFL CIRCUITS REDUCE MECP2 MRNA TO ENDOGENOUS LEVELS
IN MOUSE BRAINS

Maximizing therapeutic efficacy and safety in Rett syndrome gene therapy requires expressing AAV-delivered *Mecp2* at appropriate levels in the brain. While the precise therapeutic window of *Mecp2* expression is unknown, it presumably spans the endogenous expression range. We therefore sought to quantitatively compare expression of AAV-delivered *Mecp2* with endogenous *Mecp2* in mouse brains. To distinguish ectopic and endogenous transcripts, we designed two sets of orthogonal hybridization chain reaction (HCR) probes: one set targeted the EGFP sequence exclusive to the ectopic transcript, while the other set targeted sequences in the 3' UTR of the major isoforms of *Mecp2* that are exclusive to the endogenous gene (**Figure 3A**).

To achieve brain-specific delivery, we took advantage of a recently developed AAV capsid variant, Cap.B22, which efficiently targets the brain when systemically delivered, while de-targeting the liver and other organs (Goertsen et al. 2022). We packaged each of the constructs in Cap.B22. To compare circuit-regulated expression to that produced by a typical promoter commonly used in gene therapy (Huichalaf et al. 2022, Perdomini et al. 2014, Hocquemiller et al. 2016), we also packaged a CAG-GFP construct based on the synthetic CAG promoter. We then systemically injected each variant into WT mice at a dose of 5×10^{12} viral genomes (vg) per mouse. 3 weeks post-injection, we collected brain sections and analyzed mRNA levels using HCR and confocal microscopy (**Figure 3A, Methods**). In the resulting images, the highest expression of *Mecp2* mRNA and protein was seen in brains that received the CAG-GFP construct, followed by the unregulated, 1x, and 4x constructs in that order (**Figure 3D**).

To quantify the effect of the circuit in single cells, we segmented cells based on oligo-dT fluorescence (**Figure 3D**, second row) and counted individual transcripts within individual cells (**Methods**). The CAG-GFP construct overexpressed the ectopic transcript by a median factor of 54-fold relative to endogenous *Mecp2* (**Figure 3B**, first panel), indicating that standard synthetic promoters can greatly overexpress *Mecp2*.

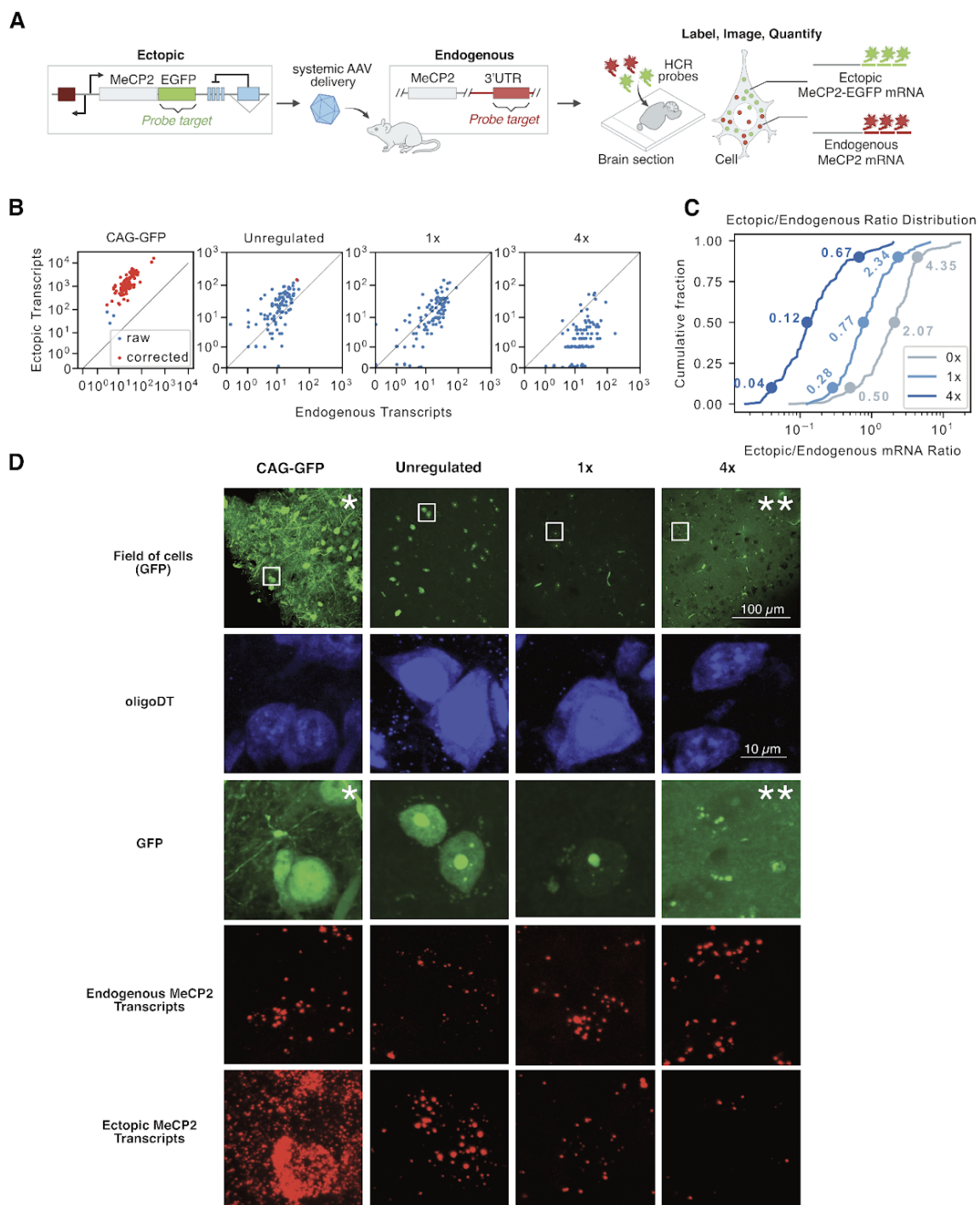


Figure 3. Synthetic miRNA IFFLs regulate expression to near or below endogenous *Mecp2* levels in mouse brains.

(A) Orthogonal HCR probes were designed to specifically target endogenous or ectopic *Mecp2*. Ectopic *Mecp2-EGFP* was targeted with HCR probes against the EGFP coding sequence. Endogenous *Mecp2* was targeted with HCR probes against sequences in the endogenous 3' UTR which do not appear in the ectopic construct. Mice were injected with viral constructs and, after 3 weeks of expression, brain slices were analyzed by HCR and confocal microscopy.

(B) Ectopic (y-axis) vs endogenous (x-axis) transcripts measured in single cells (**Methods**). The diagonal black line denotes equal expression. Red dots denote cells whose counts have been corrected to account for dense dot spacing (**Methods, Supplementary Figure 3**). *CAG-EGFP* expressed ectopic transcript at levels an order of magnitude greater than endogenous *Mecp2* transcripts. The unregulated, 1x, and 4x constructs showed progressively reduced ectopic expression, with the 1x construct matching endogenous *Mecp2* transcript levels, and the 4x construct expressing lower levels.

(C) Distributions of the ectopic to endogenous *Mecp2* transcripts in single cells. Annotations denote the 10th, 50th and 90th percentiles. The median cell receiving the unregulated construct overexpressed ectopic *Mecp2* by a factor of 2.1 relative to endogenous levels. With the 1x circuit, the median cell expressed ectopic *Mecp2* at 0.8 times the endogenous level. However, 10% of cells overexpressed ectopic *Mecp2* by a factor of at least 2.3. The median cell receiving the 4x construct only expressed 0.14 ectopic transcripts per endogenous transcript, but few cells overexpressed *Mecp2*.

(D) Sample HCR images, focusing on individual cells in a field of cortical neurons (first row, white boxes denote enlarged areas below). All cells exhibited similar endogenous *Mecp2* expression (fourth row), but decreasing ectopic MeCP2-EGFP protein (third row) and ectopic *Mecp2* transcripts (fifth row) from CAG-GFP to unregulated to 1x to 4x constructs. (*) Brightness of CAG-GFP image has been reduced to better distinguish cells. (**) Brightness of the 4x-GFP image has been increased to make the dimmer fluorescence of MeCP2 nuclear puncta more visible.

The unregulated, 1x, and 4x constructs all exhibited distinct behaviors. The unregulated construct overexpressed *Mecp2*, but to a lesser extent than CAG-GFP, with the median cell expressing 2-fold more ectopic than endogenous transcripts (**Figure 3B**, second panel, **Figure 3C**). Since even

mild overexpression of MeCP2 was previously found to be harmful (*19*), this could potentially lead to toxicity. Interestingly, the 1x construct matched the expression of *Mecp2* quite well at the median of the distribution, with 0.77 ectopic transcripts expressed per endogenous transcript. However, a tail of ~10% of cells exhibited at least 2.3-fold more ectopic than endogenous transcripts (**Figure 3B**, third panel, **Figure 3C**). By contrast, the 4x construct underexpressed *Mecp2* at the median (ectopic:endogenous ratio = 0.12) and did not exhibit a tail of overexpressing cells (**Figure 3B**, fourth panel, **Figure 3C**). The 4x circuit thus ensured that nearly the entire distribution was at or below the endogenous level. Few transcripts were measured in the negative control condition, where primary HCR probes were not added, with 48% of cells expressing one or zero counts of both transcripts (**Supplementary Figure 2**).

These results indicate that the IFFL circuits can regulate *Mecp2* expression within the mouse brain, and can achieve expression levels comparable to or less than that of endogenous *Mecp2*. They also reveal that different construct designs can generate distinct distributions of relative expression levels. Finally, they provoke the critical question of how these different distributions may ultimately impact disease progression in a model organism.

CIRCUIT-REGULATED AAV-MECP2 OUTPERFORMS UNREGULATED AAV-MECP2 IN A MOUSE MODEL OF RETT SYNDROME

To assess whether regulating the expression of AAV-delivered *Mecp2* improves behavioral outcomes in Rett model mice compared to unregulated gene therapy, we evaluated the impact of the three constructs in a mouse line carrying a *Mecp2*-null allele (Guy et al. 2001). To quantify outcomes, we used the standardized Rett phenotype score, which is based on several motor phenotypes, including hindlimb clasping and gait analysis (**Methods**) (Guy et al. 2007). Female *Mecp2*^{-X} mice were divided into 4 groups (n5): treated with the unregulated, 1x, or 4x constructs or left uninjected. At 4 weeks of age, baseline Rett phenotype scores were recorded. Mice were then systemically injected with AAV-CAP.B22-packaged constructs at a dose of 10¹⁴ vg/kg. The

Rett phenotype score was then measured biweekly until the mice reached 28 weeks of age (**Figure 4A**).

We observed an increase in phenotypic markers (hindlimb clasping and abnormal gait) in untreated female mice, but not in their wildtype littermates (**Methods, Figure 4B,C**). The mice that received unregulated *Mecp2* exhibited a similar motor phenotype to the untreated *Mecp2*^{-X} animals, potentially due to *Mecp2* overexpression-induced toxicity (**Figure 4B,C**) (Collins et al. 2004). The 1x construct produced a mild improvement in symptoms, suggesting that limiting *Mecp2* expression can reduce toxicity (**Figure 4B,C**). Strikingly, the mice that received the tightly regulated (4x) *Mecp2* performed more comparably to WT controls than the other constructs (**Figure 4B,C**), with time-averaged behavior scores significantly lower than those of both the uninjected mice (bootstrap $p = 0.003$) and the mice that received the unregulated construct (bootstrap $p = 0.01$) (**Figure 4D**). Similar significant differences were found at individual timepoints, including week 22 (**Supplementary Figure 4A**) and week 28 (**Supplementary Figure 4B**). Notably, the standard deviation of the time-averaged scores for the 4x construct, 0.30, was also significantly lower than that of the unregulated construct, 1.04 (bootstrap, $p=0.02$), demonstrating that the regulated gene therapy causes a less variable phenotype score. These results demonstrate that tighter regulation improves the efficacy of AAV-delivered *Mecp2* in mitigating progression of the Rett phenotype in female *Mecp2*^{-X} mice.

Not all phenotypes of the Rett mouse model were improved by this gene therapy. Notably, female Rett model mice have an obesity phenotype that was not significantly affected by any of the injected constructs (**Supplementary Figure 5**). Additionally, we assessed whether regulation of *Mecp2* expression could confer any benefit to *Mecp2*-null male mice, which express no MeCP2 in the brain and have a much more severe phenotype, including a 12-week lifespan. However, we found no extension of the lifespan of male *Mecp2*-null male mice in any condition (**Supplementary Figure 6**). This contrasts with modest lifespan extensions reported with other Rett syndrome gene therapies (Gadalla et al. 2017), and with the strong behavioral results in the

female mice in this work. Thus, while the regulated-*Mecp2* construct achieved strong phenotypic improvements in females without toxicity, it does not fully address all Rett phenotypes.

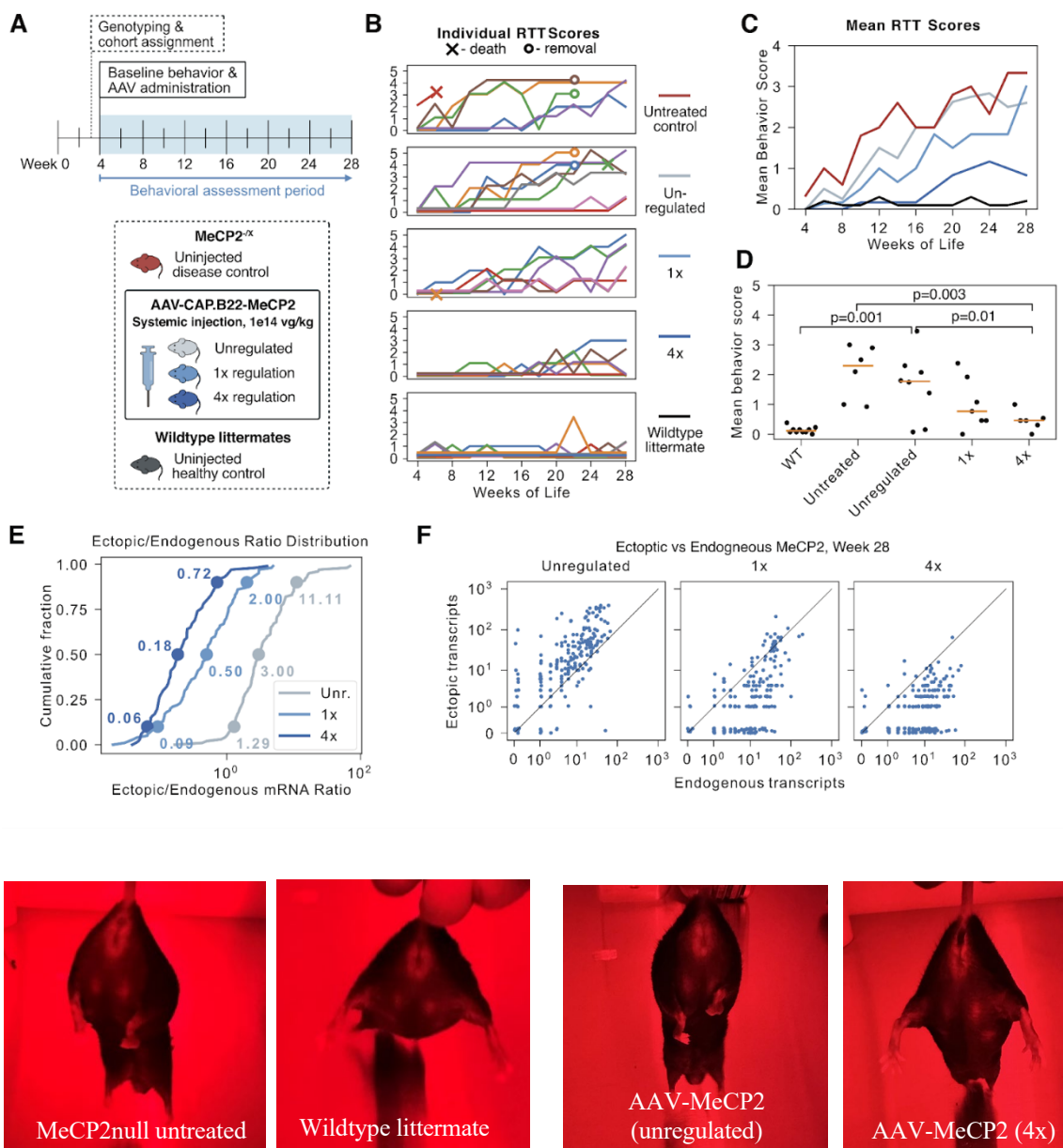


Figure 4. IFFL-regulated gene therapy outperforms unregulated gene therapy in a mouse model of Rett syndrome.

(A) Female *Mecp2*^{-X} mice were divided into 4 treatment groups: uninjected or injected with one of the 3 constructs (**Figure 2A**) packaged in AAV-CAP.B22. Female wildtype littermates were included as healthy controls. At 4 weeks of age, baseline Rett behavior scores were recorded and the mice were injected with 1×10^{14} vg/kg. Rett phenotype scores (*21*) were then measured biweekly for 24 weeks.

(B) Rett behavior (RTT) scores over time for individual mice (colored tracks) in each group. In each of the uninjected control, unregulated, and 1x groups, 1 mouse died during the study (“X” marker). In the 4x and wildtype groups, no mice died. After 22 weeks, 2 mice were removed from both the uninjected control group and the unregulated group for another experiment (“O” marker).

(C) Mean score trajectories for each group in (B). Legend in left column of (B).

(D) Rett behavior scores averaged across all timepoints for each mouse. Orange bars denote the median of each group. Mice that received the 4x construct had mean scores significantly lower than both the uninjected mice (bootstrap $p=0.003$) and mice that received the unregulated construct (bootstrap $p=0.01$). The standard deviation of the 4x group, 0.30, was also significantly lower than that of the unregulated group, 1.04 (bootstrap $p=0.02$). The mean scores of the wildtype controls were significantly lower than the uninjected controls (bootstrap $p=0.0003$) and mice receiving the unregulated (bootstrap $p=0.001$) and the 4x (bootstrap $p=0.01$) constructs.

(E) Ectopic vs endogenous *Mecp2* transcripts quantified in single cells of mouse brains after behavior experiments were completed (week 28). Brain slices were analyzed by HCR as in Figure 3. Despite continuous expression for 24 weeks, ectopic and endogenous levels remained similar for each construct.

(F) Distribution of the ratios of ectopic to endogenous transcripts in single cells after 24 weeks of expression (cf. Figure 3C). The unregulated construct overexpressed *Mecp2* by a factor of 3 at the median, while the 1x construct roughly agreed at the median, but overexpressed in the tail. The 4x construct was expressed below endogenous levels at the median, with fewer overexpressing cells.

(G) Example photos of the hindlimb clasping score component of the RTT score.

Ectopic constructs are potentially subject to unintended regulation or epigenetic silencing that could impact their operation over time. To check for such effects, we repeated the HCR analysis on the brains of mice that had finished the behavioral testing and had expressed the constructs for more than 24 weeks. All three constructs exhibited similar expression profiles as they did in the

initial analysis (**Figure 3**). Specifically, the unregulated construct produced an expression distribution whose median cell overexpressed *Mecp2* 3-fold (**Figure 4E,F**). The 1x construct matched endogenous expression better at the median (0.5-fold), but exhibited a tail of ~10% of cells overexpressing *Mecp2* at least 2-fold (**Figure 4E,F**). The 4x construct underexpressed *Mecp2*, and did not exhibit a tail of overexpressing cells (**Figure 4E,F**). Thus, the constructs maintained their expression profiles robustly through the 24 weeks of the study.

These results demonstrate that a tightly regulating synthetic miRNA IFFL can significantly augment a gene therapy for Rett syndrome in a Rett mouse model, and maintain the regulated level of expression over periods of at least 24 weeks.

Discussion

Without regulation, therapeutic genes are expressed at varying degrees across cells, which could range from insufficient to toxic levels (**Figure 1**). Here, we designed and optimized a compact synthetic miRNA-based incoherent feedforward loop circuit that can compensate for variations in gene dosage and other sources of expression variation to ensure that total mRNA and protein expression remains within a therapeutic window (**Figure 2**). When incorporated in an AAV vector, the circuit maintained expression in mouse brains at or below the level of endogenous *Mecp2* (**Figure 3**). In the context of MeCP2 gene therapy, the tightly regulated (“4x”) circuit variant rescued behavioral phenotypes in a Rett female mouse model, outperforming unregulated and more weakly regulated constructs (**Figure 4**). This work benefited from a brain-targeting systemic AAV capsid, Cap.B22 (Goertsen et al. 2022), which allows higher viral titers because it avoids delivery to the liver, where toxicity has been observed in previous studies (Gadalla et al. 2017). However, comparison between unregulated and regulated circuit variants shows that the circuit provides additional benefit beyond that achieved by capsid targeting alone. The synthetic miRNA IFFL circuits could thus improve gene therapy for Rett syndrome, and potentially other genetic disorders as well.

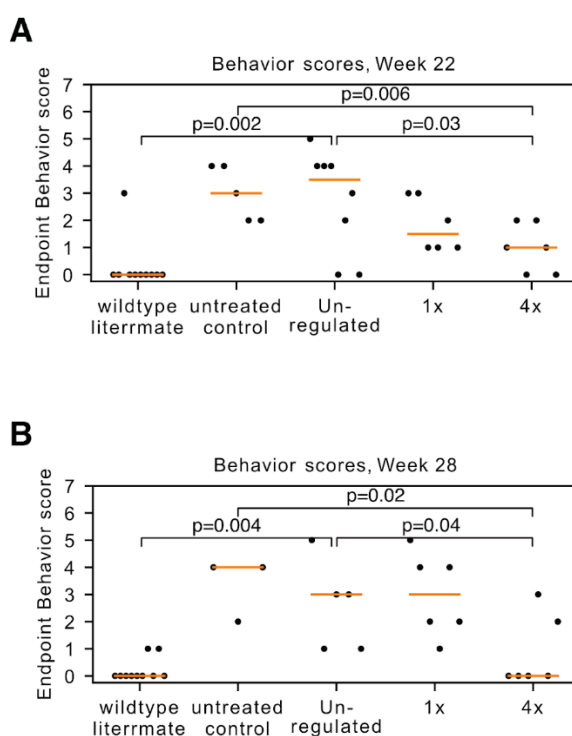
In gene therapy for Rett syndrome and other diseases, expression level is critically important. The single-molecule analysis employed here enabled us to quantitatively compare ectopic and endogenous expression levels in the same cell. This showed that a moderately regulated circuit (“1x”) closely matched endogenous mRNA levels in the median cell, but also generated a subpopulation of cells with much higher levels (**Figure 3C**). By contrast, a tightly regulated circuit (“4x”) exhibited expression lower than endogenous *Mecp2* in most cells but also avoided appreciable overexpression. The superior performance of the tightly regulated circuit in rescuing the Rett phenotype (**Figure 4B**) likely reflects this lack of high expression. Additionally, we note that both circuits reduced expression in the brain to levels far lower than that of a CAG-GFP construct, which used a more typical synthetic promoter (**Figure 3B**).

This regulated *Mecp2* gene therapy has some limitations: it did not improve the survival of male *Mecp2*-null mice and did not affect the obesity phenotype of heterozygous females. This may be due to our choice of a central nervous system (CNS)-targeting capsid. MeCP2 expression outside the CNS may be important for development and survival. Several Rett phenotypes in humans, including breathing irregularities, cardiovascular dysfunction, and decreased pain sensitivity (Weaving et al. 2021), implicate the peripheral nervous system (PNS). Future studies applying the gene therapy to the PNS and other tissues with targeted AAVs (Chen et al. 2022) could help to improve efficacy and clarify the role of MeCP2 in non-CNS cells. Additionally, the IFFL circuits introduced here do not incorporate post-transcriptional or dynamic regulation that may occur in natural MeCP2 regulation. However, the distribution of endogenous *Mecp2* mRNA appeared relatively uniform and stable over time (**Supplementary Figure 7**), suggesting that such effects may be modest in the brain.

The simplicity and compactness of the IFFL circuit make it potentially broadly useful for AAV-based gene therapies for other genetic diseases, such as SMA, Angelman syndrome, fragile X syndrome, and monogenic autism spectrum disorders (Weuring et al. 2021). The dosage compensation circuit could also extend the durability of gene therapies, by permitting higher initial vector copy numbers, and therefore a longer duration of therapeutic protein expression, while

avoiding overexpression, in dividing, diluting cells. The miRNA-based circuits used here could also improve safety and efficacy of other therapies based on ectopic expression, such as gene editing. More generally, these results suggest that synthetic circuits could play a vital role in gene therapies and other emerging therapeutic approaches.

Supplementary Figures

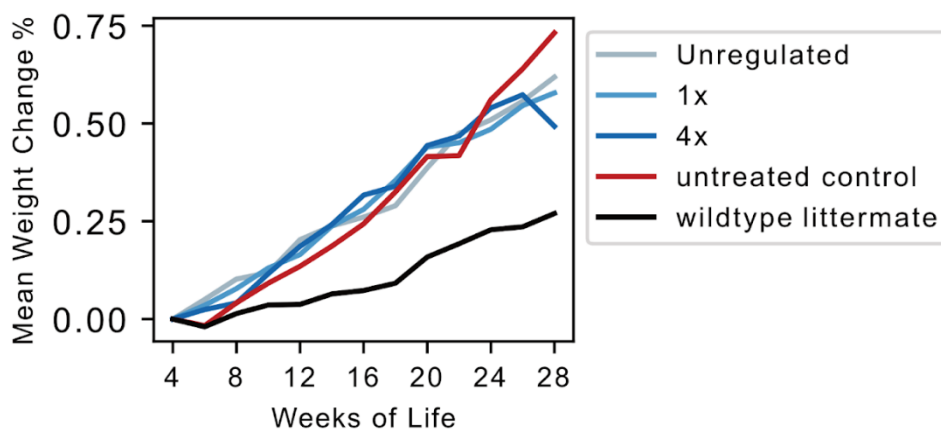


Supplementary Figure 5: Endpoint behavior score statistics

Supplementary Figure 5. Endpoint behavior score statistics.

(A) Endpoint Rett behavior scores at week 22. Mice that received the 4x construct scored significantly lower on average than both the uninjected mice (bootstrap $p=0.006$) and the mice that received the unregulated construct (bootstrap $p=0.03$). The standard deviation of the 4x group's scores, 0.82, was significantly lower than the standard deviation of the unregulated group's scores, 1.79 (bootstrap $p=0.03$). Wildtype littermates scored significantly lower than the uninjected controls (bootstrap $p=0.001$) and mice that received the unregulated construct (bootstrap $p=0.002$). The wildtype and 4x mice were not significantly different (bootstrap $p=0.08$).

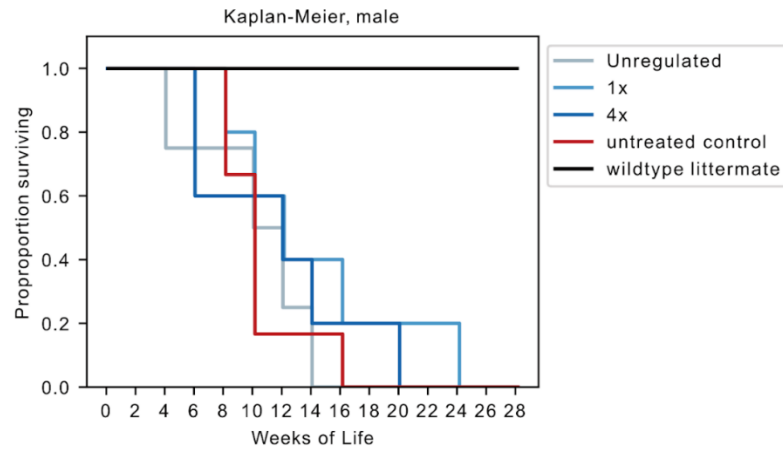
(B) Endpoint Rett behavior scores at week 28. Mice that received the 4x construct scored significantly lower on average than both the uninjected mice (bootstrap $p=0.02$) and the mice that received the unregulated construct (bootstrap $p=0.04$). The standard deviation of the 4x scores, 1.21, was not significantly lower than the standard deviation of the unregulated scores, 1.49 (bootstrap $p=0.29$). Wildtype littermates scored significantly lower than the uninjected control (bootstrap $p=0.002$) and mice receiving the unregulated construct (bootstrap $p=0.004$). The scores of wildtype and 4x mice were not significantly different (bootstrap $p=0.08$).



Supplementary Figure 6: Mouse Weight not improved

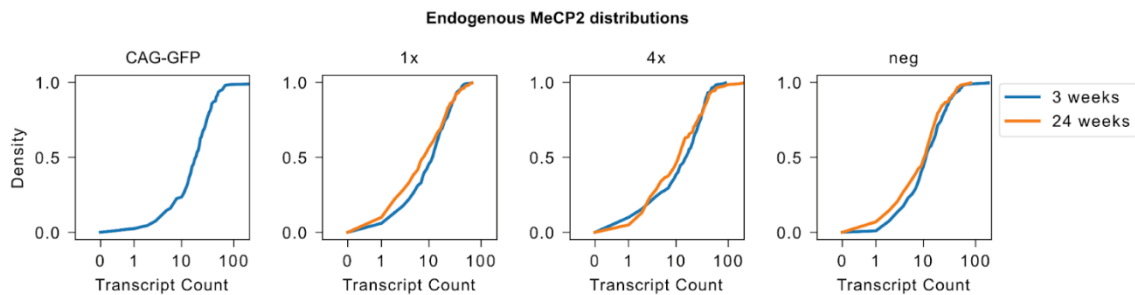
Supplementary Figure 6. Mouse weight was not affected by AAV-MeCP2 gene therapy.

Mouse weight percentage change over time for each cohort. The wildtype mouse cohort had a reduced weight relative to other cohorts, which increased similarly over time, indicating that the obesity phenotype was not affected by AAV-MeCP2 gene therapy.



Supplementary Figure 7: Male Rett Phenotype not relieved by gene therapy

Supplementary Figure 7. Male survival was not affected by AAV-MeCP2 gene therapy.
Kaplan-Meier survival curves show no significant change in lifespan in male Rett mice in any treatment group.



Supplementary Figure 4: Endogenous MeCP2 distributions

Supplementary Figure 4. Endogenous MeCP2 distribution after 3 and 24 weeks of viral expression.
Empirical cumulative distributions of endogenous *Mecp2* in mice that received different viral constructs were remarkably consistent between constructs and between 3 and 24 weeks of expressing the viral constructs.

CHAPTER 3 REFERENCES

- Pachitariu, M., and Stringer, C. (2022). Cellpose 2.0: how to train your own model. *Nat. Methods* *19*, 1634–1641.
- Stringer, C., Wang, T., Michaelos, M., and Pachitariu, M. (2021). Cellpose: a generalist algorithm for cellular segmentation. *Nat. Methods* *18*, 100–106.
- Collins, B.E., Merritt, J.K., Erickson, K.R., and Neul, J.L. (2022). Safety and efficacy of genetic MECP2 supplementation in the R294X mouse model of Rett syndrome. *Genes Brain Behav.* *21*, e12739.
- Du, R., Flynn, M.J., Honsa, M., Jungmann, R., and Elowitz, M.B. (2024). miRNA circuit modules for precise, tunable control of gene expression. *bioRxiv*. 10.1101/2024.03.12.583048.
- Love, M.I., Huber, W., and Anders, S. (2014). Moderated estimation of fold change and dispersion for RNA-seq data with DESeq2. *Genome Biol.* *15*, 550.
- Gillespie, D.T. (1977). Exact stochastic simulation of coupled chemical reactions. *J. Phys. Chem.* *81*, 2340–2361.
- Benger, M., Kinali, M., and Mazarakis, N.D. (2018). Autism spectrum disorder: prospects for treatment using gene therapy. *Mol. Autism* *9*, 39.
- Weuring, W., Geerligs, J., and Koeleman, B.P.C. (2021). Gene Therapies for Monogenic Autism Spectrum Disorders. *Genes* *12*. 10.3390/genes12111667.
- Chen, X., Ravindra Kumar, S., Adams, C.D., Yang, D., Wang, T., Wolfe, D.A., Arokiaraj, C.M., Ngo, V., Campos, L.J., Griffiths, J.A., et al. (2022). Engineered AAVs for non-invasive gene delivery to rodent and non-human primate nervous systems. *Neuron* *110*, 2242–2257.e6.

Weaving, L.S., Ellaway, C.J., Gécz, J., and Christodoulou, J. (2005). Rett syndrome: clinical review and genetic update. *J. Med. Genet.* 42, 1–7.

Hocquemiller, M., Giersch, L., Audrain, M., Parker, S., and Cartier, N. (2016). Adeno-Associated Virus-Based Gene Therapy for CNS Diseases. *Hum. Gene Ther.* 27, 478–496.

Takei, Y., Zheng, S., Yun, J., Shah, S., Pierson, N., White, J., Schindler, S., Tischbirek, C.H., Yuan, G.-C., and Cai, L. (2021). Single-cell nuclear architecture across cell types in the mouse brain. *Science* 374, 586–594.

Fellmann, C., Hoffmann, T., Sridhar, V., Hopfgartner, B., Muhar, M., Roth, M., Lai, D.Y., Barbosa, I.A.M., Kwon, J.S., Guan, Y., et al. (2013). An optimized microRNA backbone for effective single-copy RNAi. *Cell Rep.* 5, 1704–1713.

Qiu, L., Wang, H., Xia, X., Zhou, H., and Xu, Z. (2008). A construct with fluorescent indicators for conditional expression of miRNA. *BMC Biotechnol.* 8, 77.

Megraw, M., Sethupathy, P., Gumireddy, K., Jensen, S.T., Huang, Q., and Hatzigeorgiou, A.G. (2010). Isoform specific gene auto-regulation via miRNAs: a case study on miR-128b and ARPP-21. *Theor. Chem. Acc.* 125, 593–598.

Tsang, J., Zhu, J., and van Oudenaarden, A. (2007). MicroRNA-mediated feedback and feedforward loops are recurrent network motifs in mammals. *Mol. Cell* 26, 753–767.

Chamorro-Jorganes, A., Araldi, E., Rotllan, N., Cirera-Salinas, D., and Suárez, Y. (2014). Autoregulation of glypican-1 by intronic microRNA-149 fine tunes the angiogenic response to FGF2 in human endothelial cells. *J. Cell Sci.* 127, 1169–1178.

Khammash, M.H. (2021). Perfect adaptation in biology. *Cell Syst* *12*, 509–521.

Strovas, T.J., Rosenberg, A.B., Kuypers, B.E., Muscat, R.A., and Seelig, G. (2014). MicroRNA-based single-gene circuits buffer protein synthesis rates against perturbations. *ACS Synth. Biol.* *3*, 324–331.

Frei, T., Cella, F., Tedeschi, F., Gutiérrez, J., Stan, G.-B., Khammash, M., and Siciliano, V. (2020). Characterization and mitigation of gene expression burden in mammalian cells. *Nat. Commun.* *11*, 4641.

Osella, M., Bosia, C., Corá, D., and Caselle, M. (2011). The role of incoherent microRNA-mediated feedforward loops in noise buffering. *PLoS Comput. Biol.* *7*, e1001101.

Jones, R.D., Qian, Y., Siciliano, V., DiAndreth, B., Huh, J., Weiss, R., and Del Vecchio, D. (2020). An endoribonuclease-based feedforward controller for decoupling resource-limited genetic modules in mammalian cells. *Nat. Commun.* *11*, 5690.

Lillacci, G., Benenson, Y., and Khammash, M. (2018). Synthetic control systems for high performance gene expression in mammalian cells. *Nucleic Acids Res.* *46*, 9855–9863.

Segall-Shapiro, T.H., Sontag, E.D., and Voigt, C.A. (2018). Engineered promoters enable constant gene expression at any copy number in bacteria. *Nat. Biotechnol.* *36*, 352–358.

Bleris, L., Xie, Z., Glass, D., Adadey, A., Sontag, E., and Benenson, Y. (2011). Synthetic incoherent feedforward circuits show adaptation to the amount of their genetic template. *Mol. Syst. Biol.* *7*, 519.

Mangan, S., and Alon, U. (2003). Structure and function of the feed-forward loop network motif. *Proc. Natl. Acad. Sci. U. S. A.* *100*, 11980–11985.

Frei, T., and Khammash, M. (2021). Adaptive circuits in synthetic biology. *Current Opinion in Systems Biology* 28, 100399.

Tillotson, R., Selfridge, J., Koerner, M.V., Gadalla, K.K.E., Guy, J., De Sousa, D., Hector, R.D., Cobb, S.R., and Bird, A. (2017). Radically truncated MeCP2 rescues Rett syndrome-like neurological defects. *Nature* 550, 398–401.

Prasad, K.-M.R., Xu, Y., Yang, Z., Acton, S.T., and French, B.A. (2011). Robust cardiomyocyte-specific gene expression following systemic injection of AAV: in vivo gene delivery follows a Poisson distribution. *Gene Ther.* 18, 43–52.

Wang, S.K., Lapan, S.W., Hong, C.M., Krause, T.B., and Cepko, C.L. (2020). In Situ Detection of Adeno-associated Viral Vector Genomes with SABER-FISH. *Mol Ther Methods Clin Dev* 19, 376–386.

Nathwani, A.C., Rosales, C., McIntosh, J., Rastegarlar, G., Nathwani, D., Raj, D., Nawathe, S., Waddington, S.N., Bronson, R., Jackson, S., et al. (2011). Long-term safety and efficacy following systemic administration of a self-complementary AAV vector encoding human FIX pseudotyped with serotype 5 and 8 capsid proteins. *Mol. Ther.* 19, 876–885.

Matagne, V., Ehinger, Y., Saidi, L., Borges-Correia, A., Barkats, M., Bartoli, M., Villard, L., and Roux, J.-C. (2017). A codon-optimized *Mecp2* transgene corrects breathing deficits and improves survival in a mouse model of Rett syndrome. *Neurobiol. Dis.* 99, 1–11.

Gadalla, K.K.E., Bailey, M.E.S., Spike, R.C., Ross, P.D., Woodard, K.T., Kalburgi, S.N., Bachaboina, L., Deng, J.V., West, A.E., Samulski, R.J., et al. (2013). Improved survival and reduced phenotypic severity following AAV9/MECP2 gene transfer to neonatal and juvenile male *Mecp2* knockout mice. *Mol. Ther.* 21, 18–30.

Ramocki, M.B., Peters, S.U., Tavyev, Y.J., Zhang, F., Carvalho, C.M.B., Schaaf, C.P., Richman, R., Fang, P., Glaze, D.G., Lupski, J.R., et al. (2009). Autism and other neuropsychiatric symptoms are prevalent in individuals with MeCP2 duplication syndrome. *Ann. Neurol.* *66*, 771–782.

Collins, A.L., Levenson, J.M., Vilaythong, A.P., Richman, R., Armstrong, D.L., Noebels, J.L., David Sweatt, J., and Zoghbi, H.Y. (2004). Mild overexpression of MeCP2 causes a progressive neurological disorder in mice. *Hum. Mol. Genet.* *13*, 2679–2689.

Tropea, D., Giacometti, E., Wilson, N.R., Beard, C., McCurry, C., Fu, D.D., Flannery, R., Jaenisch, R., and Sur, M. (2009). Partial reversal of Rett Syndrome-like symptoms in MeCP2 mutant mice. *Proc. Natl. Acad. Sci. U. S. A.* *106*, 2029–2034.

Hagberg, B., Aicardi, J., Dias, K., and Ramos, O. (1983). A progressive syndrome of autism, dementia, ataxia, and loss of purposeful hand use in girls: Rett's syndrome: report of 35 cases. *Ann. Neurol.* *14*, 471–479.

Villard, L., Kpebe, A., Cardoso, C., Chelly, P.J., Tardieu, P.M., and Fontes, M. (2000). Two affected boys in a Rett syndrome family: clinical and molecular findings. *Neurology* *55*, 1188–1193.

Tillotson, R., and Bird, A. (2020). The Molecular Basis of MeCP2 Function in the Brain. *J. Mol. Biol.* *432*, 1602–1623.

Amir, R., Veyver, I.V.D., Wan, M., Tran, C.Q., Francke, U., and Zoghbi, H. (1999). Rett syndrome is caused by mutations in X-linked MECP2, encoding methyl-CpG-binding protein 2. *Nat. Genet.* *23*, 185–188.

Hordeaux, J., Buza, E.L., Dyer, C., Goode, T., Mitchell, T.W., Richman, L., Denton, N., Hinderer,

C., Katz, N., Schmid, R., et al. (2020). Adeno-Associated Virus-Induced Dorsal Root Ganglion Pathology. *Hum. Gene Ther.* 31, 808–818.

Van Alstyne, M., Tattoli, I., Delestrée, N., Recinos, Y., Workman, E., Shihabuddin, L.S., Zhang, C., Mentis, G.Z., and Pellizzoni, L. (2021). Gain of toxic function by long-term AAV9-mediated SMN overexpression in the sensorimotor circuit. *Nat. Neurosci.* 24, 930–940.

Smith, S.E.P., Zhou, Y.-D., Zhang, G., Jin, Z., Stoppel, D.C., and Anderson, M.P. (2011). Increased gene dosage of Ube3a results in autism traits and decreased glutamate synaptic transmission in mice. *Sci. Transl. Med.* 3, 103ra97.

Mendell, J.R., Al-Zaidy, S.A., Rodino-Klapac, L.R., Goodspeed, K., Gray, S.J., Kay, C.N., Boye, S.L., Boye, S.E., George, L.A., Salabarria, S., et al. (2021). Current Clinical Applications of In Vivo Gene Therapy with AAVs. *Mol. Ther.* 29, 464–488.

Russell, S., Bennett, J., Wellman, J.A., Chung, D.C., Yu, Z.-F., Tillman, A., Wittes, J., Pappas, J., Elci, O., McCague, S., et al. (2017). Efficacy and safety of voretigene neparvovec (AAV2-hRPE65v2) in patients with RPE65-mediated inherited retinal dystrophy: a randomised, controlled, open-label, phase 3 trial. *Lancet* 390, 849–860.

Ozelo, M.C., Mahlangu, J., Pasi, K.J., Giermasz, A., Leavitt, A.D., Laffan, M., Symington, E., Quon, D.V., Wang, J.-D., Peerlinck, K., et al. (2022). Valoctocogene Roxaparvovec Gene Therapy for Hemophilia A. *N. Engl. J. Med.* 386, 1013–1025.

George, L.A., Sullivan, S.K., Giermasz, A., Rasko, J.E.J., Samelson-Jones, B.J., Ducore, J., Cuker, A., Sullivan, L.M., Majumdar, S., Teitel, J., et al. (2017). Hemophilia B Gene Therapy with a High-Specific-Activity Factor IX Variant. *N. Engl. J. Med.* 377, 2215–2227.

Nathwani, A.C., Reiss, U.M., Tuddenham, E.G.D., Rosales, C., Chowdary, P., McIntosh, J., Della

Peruta, M., Lheriteau, E., Patel, N., Raj, D., et al. (2014). Long-term safety and efficacy of factor IX gene therapy in hemophilia B. *N. Engl. J. Med.* *371*, 1994–2004.

Mendell, J.R., Al-Zaidy, S., Shell, R., Arnold, W.D., Rodino-Klapac, L.R., Prior, T.W., Lowes, L., Alfano, L., Berry, K., Church, K., et al. (2017). Single-Dose Gene-Replacement Therapy for Spinal Muscular Atrophy. *N. Engl. J. Med.* *377*, 1713–1722.

Hinderer, C., Katz, N., Buza, E.L., Dyer, C., Goode, T., Bell, P., Richman, L.K., and Wilson, J.M. (2018). Severe Toxicity in Nonhuman Primates and Piglets Following High-Dose Intravenous Administration of an Adeno-Associated Virus Vector Expressing Human SMN. *Hum. Gene Ther.* *29*, 285–298.

Challis, R.C., Ravindra Kumar, S., Chen, X., Goertsen, D., Coughlin, G.M., Hori, A.M., Chuapoco, M.R., Otis, T.S., Miles, T.F., and Gradinaru, V. (2022). Adeno-Associated Virus Toolkit to Target Diverse Brain Cells. *Annu. Rev. Neurosci.* *45*, 447–469.

Perdomini, M., Belbellaa, B., Monassier, L., Reutenauer, L., Messaddeq, N., Cartier, N., Crystal, R.G., Aubourg, P., and Puccio, H. (2014). Prevention and reversal of severe mitochondrial cardiomyopathy by gene therapy in a mouse model of Friedreich's ataxia. *Nat. Med.* *20*, 542–547.

Huichalaf, C., Perfitt, T.L., Kuperman, A., Gooch, R., Kovi, R.C., Brenneman, K.A., Chen, X., Hirehallur-Shanthappa, D., Ma, T., Assaf, B.T., et al. (2022). In vivo overexpression of frataxin causes toxicity mediated by iron-sulfur cluster deficiency. *Mol Ther Methods Clin Dev* *24*, 367–378.

Sinnett, S.E., Boyle, E., Lyons, C., and Gray, S.J. (2021). Engineered microRNA-based regulatory element permits safe high-dose miniMECP2 gene therapy in Rett mice. *Brain* *144*, 3005–3019.

Powers, S., Likhite, S., Gadalla, K.K., Miranda, C.J., Hufferberger, A.J., Dennys, C., Foust, K.D.,

Morales, P., Pierson, C.R., Rinaldi, F., et al. (2023). Novel MECP2 gene therapy is effective in a multicenter study using two mouse models of Rett syndrome and is safe in non-human primates. *Mol. Ther.* *31*, 2767–2782.

Guy, J., Gan, J., Selfridge, J., Cobb, S., and Bird, A. (2007). Reversal of neurological defects in a mouse model of Rett syndrome. *Science* *315*, 1143–1147.

Matagne, V., Borloz, E., Ehinger, Y., Saidi, L., Villard, L., and Roux, J.-C. (2021). Severe off-target effects following intravenous delivery of AAV9-MECP2 in a female mouse model of Rett syndrome. *Neurobiol. Dis.* *149*, 105235.

Sinnett, S.E., Hector, R.D., Gadalla, K.K.E., Heindel, C., Chen, D., Zaric, V., Bailey, M.E.S., Cobb, S.R., and Gray, S.J. (2017). Improved MECP2 Gene Therapy Extends the Survival of MeCP2-Null Mice without Apparent Toxicity after Intracisternal Delivery. *Mol Ther Methods Clin Dev* *5*, 106–115.

Gadalla, K.K.E., Vudhironarit, T., Hector, R.D., Sinnett, S., Bahey, N.G., Bailey, M.E.S., Gray, S.J., and Cobb, S.R. (2017). Development of a Novel AAV Gene Therapy Cassette with Improved Safety Features and Efficacy in a Mouse Model of Rett Syndrome. *Mol Ther Methods Clin Dev* *5*, 180–190.

Guy, J., Hendrich, B., Holmes, M., Martin, J.E., and Bird, A. (2001). A mouse *Mecp2*-null mutation causes neurological symptoms that mimic Rett syndrome. *Nat. Genet.* *27*, 322–326.

Challis, R.C., Ravindra Kumar, S., Chan, K.Y., Challis, C., Beadle, K., Jang, M.J., Kim, H.M., Rajendran, P.S., Tompkins, J.D., Shivkumar, K., et al. (2019). Systemic AAV vectors for widespread and targeted gene delivery in rodents. *Nat. Protoc.* *14*, 379–414.

Chuapoco, M.R., Flytzanis, N.C., Goeden, N., Christopher Octeau, J., Roxas, K.M., Chan, K.Y.,

Scherrer, J., Winchester, J., Blackburn, R.J., Campos, L.J., et al. (2023). Adeno-associated viral vectors for functional intravenous gene transfer throughout the non-human primate brain. *Nat. Nanotechnol.* *18*, 1241–1251.

Rumbaugh, G., Adams, J.P., Kim, J.H., and Huganir, R.L. (2006). SynGAP regulates synaptic strength and mitogen-activated protein kinases in cultured neurons. *Proc. Natl. Acad. Sci. U. S. A.* *103*, 4344–4351.

Berryer, M.H., Hamdan, F.F., Klitten, L.L., Møller, R.S., Carmant, L., Schwartzenuber, J., Patry, L., Dobrzeniecka, S., Rochefort, D., Neugnot-Cerioli, M., et al. (2013). Mutations in SYNGAP1 cause intellectual disability, autism, and a specific form of epilepsy by inducing haploinsufficiency. *Hum. Mutat.* *34*, 385–394.

Goertsen, D., Flytzanis, N.C., Goeden, N., Chuapoco, M.R., Cummins, A., Chen, Y., Fan, Y., Zhang, Q., Sharma, J., Duan, Y., et al. (2022). AAV capsid variants with brain-wide transgene expression and decreased liver targeting after intravenous delivery in mouse and marmoset. *Nat. Neurosci.* *25*, 106–115.

CONCLUSION

In this thesis, I have described three strategies for achieving the true aim of gene therapies: restoring homeostasis to cells, tissues, systems and organisms that have suffered genetic insults beyond their capacity to cope with these changes, resulting in disease. The need for these delivery and regulatory technologies scales with the size of the collective patient population. Millions of people worldwide are afflicted with disorders that stem from genetic mutations and manifest as multisystem, debilitating conditions. However, as each individual disorder is challenging to bring through clinical development of tailored therapies, it is important to develop strategies that may be applied to multiple disorders in parallel, especially if they share common mechanisms, even if they are traditionally not thought of in the same class and treated by the same physicians. For example, Rett Syndrome is typically treated as an autism spectrum disorder, but the scope of disorders that suffer from the same goldilocks expression control problem span the disciplines of oncology, neurology, and several other specialties. Identification of regulatory elements and promoters that can help achieve more physiologic and specific distributions of expression can work in tandem with several delivery mechanisms, enabling custom therapies for hundreds or thousands of disorders with development of only tens of modular tools. Further, the problem of off target and unanticipated toxicities from a permanent therapy may in principle be reversible or tunable post-hoc, if we can capture the biological particulars of AAV genome biology, harnessing it as a tool. Though further work is needed to develop these tools and expand their applications, I conclude that AAV gene therapies can be made safer, more targeted, effective, and accessible with advances in these technologies.

APPENDIX A

MATERIALS AND METHODS – CHAPTER 2

AAV-FXN genome development

We constructed three candidate cDNA AAV genomes that express frataxin. Frataxin expression was either driven by the strong and ubiquitous CAG promoter or the putative FXN core promoter. Expression was validated in HEK293 cells prior to *in vivo* experimentation.

Virus production and purification

AAVs were generated as previously described (Chan 2017) using HEK293 cells (ATCC). Capsid, Genome and Helper plasmids were triple transfected into HEK293 cells using PEI-Max(____). Viral particles were harvested from the cells and media at 70 and 120 hours using 40% polyethylene glycol in 500mM NaCl and digestion with salt-active nuclease (Arcticzymes). The virus-containing supernatant was then purified using ultracentrifugation through iodixanol step gradient columns (15%, 25%, 40% and 60%). Viruses were filtered and concentrated using Amicon filters in sterile PBS. Viral titers were measured by qPCR against a standard linearized FXN containing genome.

Evaluation of construct expression *in vivo*

Animals: All *in vivo* experimentation was conducted under the approval of the Institutional Animal Care and Use Committee of the California Institute of Technology. Expression of each candidate FXN construct was validated in WT mice (C57Bl/6J, purchased from Jackson Laboratory) by immunohistochemistry as previously described (Chan 2017)(See list of antibodies). WT mice (n=4 per group, 6-8 weeks of age) were injected intravenously with AAV-PHP-CAP.B10 or AAV-PHP.PNS2 packaging the candidate FXN constructs (1-3E11 vg/mouse). After 4 weeks of expression (unless otherwise noted), mice were euthanized using EUTHASOL (Virbac) and

transcardiac perfused with PBS containing heparin, followed by cold 4% paraformaldehyde in PBS. Tissues were post-fixed overnight in 4% PFA before rinsing and transferring to PBS with 0.05% sodium azide. Tissues were sectioned on a Leica VT1200 vibratome or cryosectioned at 30 μ M on a cryostat (Leica).

Immunohistochemistry: Brain sections were incubated in blocking solution (filter sterilized 10% normal donkey serum, 0.1% Triton X-100, and 0.05% sodium azide in PBS) for one hour at room temperature prior to incubation with primary antibodies in blocking solution overnight at 4 degrees. They were then washed in PBS three times for 15 minutes each at RT. Samples were then switched to secondary antibody incubation for 4 hours at room temperature and thoroughly washed in PBS before mounting onto slides using mounting medium. Expression was quantified using the Keyence BZX microscope system. (Antibodies: anti-FLAG: 14793S, Cell Signaling and F3165, Sigma, 1:500. Anti-FXN: (ab175402, Abcam, 1:500).

Evaluating the Therapeutic Efficacy of AAV-FXN

FXN prophylactic treatment and knockdown:

A pilot cohort of FXNiKD animals was treated with AAV-PHP.CAP-B.10 and PHP.S in the post-symptomatic period. Two additional cohorts were treated using a preventative paradigm, in which the animals are treated with AAV-FXN and allowed time to express the construct (2 weeks) before we initiated knockdown of endogenous FXN. Knockdown was initiated using doxycycline hyclate in the drinking water (2 mg/mL in 5% sucrose) refreshed every 3 days, in addition to doxycycline diet (BioServ).

Behavioral testing:

Beam traversal (Fleming et al., 2013): A 1 m plexiglass beam (Stark's Plastics, Forest Park, OH) was constructed from four 0.25 m segments of narrowing widths (3.5 cm, 2.5 cm, 1.5 cm, 0.5 cm). Each segment had 1 cm overhangs placed 1 cm below the beam surface. The beam was arranged on top of empty clean cages, with the narrowest end placed inside the home cage. Animals were trained

over 2 days and 8 trials. On the third day, animals were filmed performing 3 experimental trials for later analysis. The time to traverse the beam, defined as the time between the forepaws being placed on the 2.5 cm segment and home cage, and the number of slips were quantified.

Weightlifting (Deacon, 2013): Fine-gauge stainless steel wire was formed into a loose, 3-cm-diameter ball and small, weighted C-clamps were attached to generate 7 weights: 20, 33, 46, 59, 72, 85, and 98 g. The smallest weight was designated #1 and the heaviest #7. Mice were held by the base of the tail and first positioned over weight #1 to grasp the wire ball. Once a grip was formed, the mouse was lifted until the weight was cleared from the bench top and the timer started. If the mouse held on to the weight for 3 s, an attempt to lift weight #2 was made. This was repeated until weight #7 was reached. If a mouse did not grasp a weight for 3 s, it was given 2 more opportunities to do so. A 10 s rest was given between each weight lift. The weightlifting score was determined by the formula: [(maximum weight held for 3 s) * 3] + (time holding the next heaviest weight).

ECG: Animals were anaesthetized using isoflurane gas for the duration of the procedure. Surface electrodes were positioned under the skin of the right and left forepaw and the right hindpaw to elicit a lead II pattern, and ECG measurements were recorded (AD Instruments, PowerLab and LabChart ECG analysis package) for two continuous minutes for each trial. For analysis, QT duration and waveform analysis, the 30 second section with the least electrical noise was selected and analyzed using LabChart ECG analysis (AD Instruments).

APPENDIX B

MATERIALS AND METHODS – CHAPTER 3

AAV production and purification for in vivo assessment of constructs

Plasmids used for AAV preparation include the single stranded (ss) rAAV genomes containing the cassettes described in the main text, pHelper (Addgene) and plasmids encoding AAV-CAP.B22 (Goertsen et al. 2022, Chuapoco et al. 2023). Viruses were prepared through triple-transient transfection in adherent HEK293 cell culture (ATCC) and purified by ultracentrifugation as previously described (Challis et al. 2019). Viruses were concentrated in sterile saline for injection into rodents, and viral titers were measured by qPCR.

Animals

All experiments involving animals were approved by the Institutional Animal Care and Use Committee (IACUC) and Office of Laboratory Animal Research (OLAR) at the California Institute of Technology.

The animals used in this study are the Rett syndrome model commonly known as *Mecp2*-null (Jackson Laboratories 003890). The colony was maintained on a C57Bl/6J background for compatibility with the engineered AAV capsids used in this study. Mice in behavioral cohorts were group housed when possible at 71-75°F under a reverse light cycle (12h on, 12h off) with enrichment materials such as blocks and shepherd shacks.

Intravenous AAV administration and behavioral assessment in *Mecp2*-null mice

To assess the performance of the AAV-MeCP2 candidate constructs against the disease phenotype of the *Mecp2*-null rodent model of Rett Syndrome, animals were genotyped at week 3 of life and randomized into groups controlled for sex, age and breeding pair origin. Mice in treatment groups were injected intravenously through the retro-orbital vein as previously described (Challis et al. 2019). Heterozygous females and hemizygous males were divided into balanced cohorts to receive no injection (n=12; 6 male and 6 female), or were dosed by weight to receive 1e14 viral genomes/kilogram of the AAV-CAP.B22-MeCP2 unregulated (n=13; 5 male and 8 female), 1x (1 target site; n=13; 6 male and 7 female) or 4x (4

target sites; n=11; 5 male and 6 female) *Mecp2* therapeutic constructs. These mice, along with their wildtype littermates, were assessed at baseline for motor and neurological performance using the RTT Phenotype Scoring Scale as previously described (Guy et al. 2007) and re-assessed every two weeks by a blinded researcher. Testing continued until the study end at 18 or 24 weeks post injection, or until humane endpoint criteria were reached, resulting in withdrawal of an animal from the study. All behavioral scoring was done individually in a large plastic arena outside of the home cage, and was performed during the dark phase under red light. We observed a phenotype increase earlier than some studies (Guy et al. 2007, Guy et al. 2001), but consistent with timing observed in others (Collins et al. 2022).

***Mecp2* RNA histological analysis**

Following 3 weeks of expression, injected rodents were deeply sedated via intraperitoneal injection of Euthasol (pentobarbital sodium and phenytoin sodium solution, Virbac AC) prior to cardiac perfusion using RNase-free, heparinized saline and 4% paraformaldehyde (PFA) in 0.1M phosphate buffered saline (PBS). Tissues were post-fixed in 4% PFA for 24-48 hours and either sliced on a vibratome at 50 μ M for immediate analysis or cryoprotected with RNase-free 10% and 30% sucrose solution, frozen in OCT and stored at -80°C. Prior to analysis, tissues were sliced to a thickness of 50 μ M on a Leica cryostat. Tissue slices collected for FISH analysis were incubated in ice cold RNase-free 70% ethanol prior to probing.

Hybridization chain reaction

Probes and Buffers: Probe sets were ordered from Molecular Technologies (<https://www.moleculartechnologies.org/>) against the coding sequence of EGFP and endogenous musculus *Mecp2* isoform 1 (NM_001081979), with specific instructions to only include the 3' UTR for the latter. Molecular Technologies hybridization buffer, wash buffer, and amplification buffer were included as part of the order.

Protocol: Paraformaldehyde-fixed fresh or frozen brain tissue was sliced to a thickness of 50 μ m, mounted onto glass coverslips and dried in a fume hood. Slices obtained from frozen brain tissue were rinsed with RNase-free PBS to remove OCT compound prior to drying. Ice cold RNase-free 70% ethanol was applied to the dried tissue slices. After incubating at 4 °C for 1 hour, the ethanol was removed and samples were dried in a fume hood. Once dry, the coverslips were washed with PBS before incubating in 8% SDS in PBS

for 20 minutes at room temperature. The SDS solution was then poured off and the coverslips were rinsed 3 times with PBS for 2 minutes. The area of the coverslips around the tissue slices was then dabbed dry with a Kimwipe before mounting a SecureSeal hybridization chamber (Grade Biolabs #621502) on top of the tissue slices. Using the hybridization chambers, the samples were washed with 5xSSCT (5xSSC with 0.1% Tween 20) and then the samples were pre-incubated with 30% HCR probe hybridization buffer for 30 minutes at 37 °C. After this incubation, the tissue slices were incubated with 0.2 µL of 2 µM stock of each of the odd and even HCR probe mixtures for both ectopic and endogenous target in 100 µL 30% HCR probe hybridization buffer for 3 days at 37 °C. After, the tissue slices were washed 4 times with 30% HCR probe wash buffer at 37 °C for 15 minutes. Then the tissue slices were washed twice with 5xSSCT for 5 minutes at room temperature. Next, the tissue slices were pre-incubated with HCR amplification buffer for 30 minutes at room temperature. While this was happening, for each of the 3 µM stocks of hairpins H1 and H2 for both endogenous and ectopic targets (4 total), 2µL was added to separate PCR tubes (4 total) and heated to 95 °C for 90 seconds before being allowed to cool to room temperature in a dark drawer for 30 minutes. After this was completed, the 2 µL from each of the PCR tubes was added to 100 µL of amplification buffer and the tissue slices were incubated in this solution for 90 minutes at room temperature in the dark. Once complete, the samples were washed 4 times for 15 minutes with 5xSSCT. The samples were then washed once with 2xSSC, and then the slices were incubated with 500nM oligoDT-Alexa405 in 2xSSC for 1 hour at room temperature. The samples were then washed 4 times with 2xSSC, and finally mounted in Prolong Gold (ThermoFisher #P10144).

Cell segmentation

Cell segmentation was performed using the Cellpose program (<https://www.cellpose.org/>) (Stringer et al. 2021, Pachitariu and Stringer, 2022) applied to the oligoDT signal (**Figure 3**) or a Na/K ATPase membrane marker (**Figure 2**). The basic 'cyto' model proved sufficient to accurately segment cell bodies in the vast majority of cases. The masks generated by Cellpose were then passed to the next parts of the program.

Bootstrap significance testing

To test the statistical significance of the difference between the means of two sets of samples, we followed a standard bootstrap hypothesis testing procedure. Briefly, samples from both groups were pooled into a single set. Two new sets with the same size as the original sets were then constructed by sampling with replacement from the pooled set and the means of the resampled sets were compared. This was repeated

10^5 times, and the proportion of resampled set pairs with means that differed by more than the observed difference of the original pair was reported as the p-value.